

MLBP BN C4

WL-TR-92-4004

ADA 252 118



**CHARACTERIZATION AND ANALYSIS OF DEFECTS IN  
NONLINEAR OPTICAL MOLECULAR COMPOSITE FILMS**

**Rajeev Mehta  
Adtech Systems Research Inc.  
Dayton, Ohio 45432**

**Charles Y.-C. Lee  
Polymer Branch  
Nonmetallic Materials Division**

**April 1992**

**Final Report for Period September 1989 to April 1991**

**Approved for public release; distribution is unlimited.**

**MATERIALS DIRECTORATE  
WRIGHT LABORATORY  
AIR FORCE SYSTEMS COMMAND  
WRIGHT-PATTERSON AFB, OH 45433-6533**

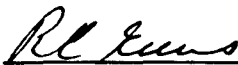
20040219163

## NOTICE

When Government drawings, specifications, or other data are used for any purpose other than in connection with a definitely Government-related procurement, the United States Government incurs no responsibility or any obligation whatsoever. The fact that the Government may have formulated or in any way supplied the said drawings, specifications, or other data, is not to be regarded by implication, or otherwise in any manner construed, as licensing the holder, or any other person or corporation; or as conveying any rights or permission to manufacture, use, or sell any patented invention that may in any way be related thereto.

This report is releasable to the National Technical Information Service (NTIS). At NTIS, it will be available to the general public including foreign nations.

This technical report has been reviewed and is approved for publication.

  
\_\_\_\_\_  
ROBERT C. EVERS, Project Scientist  
Polymer Branch  
Nonmetallic Materials Division

  
\_\_\_\_\_  
C. E. HELMINIAK, Chief  
Polymer Branch  
Nonmetallic Materials Division

  
\_\_\_\_\_  
MERRILL L. MINGES, Director  
Nonmetallic Materials Division

If your address has changed, if you wish to be removed from our mailing list, or if the addressee is no longer employed by your organization, please notify WL/MLBP, Wright-Patterson AFB, OH 45433-6533, to help us maintain a current mailing list.

Copies of this report should not be returned unless return is required by security considerations, contractual obligations, or notice on a specific document.

**REPORT DOCUMENTATION PAGE**

Form Approved  
OMB No. 0704-0188

1a. REPORT SECURITY CLASSIFICATION <b>Unclassified</b>		1b. RESTRICTIVE MARKINGS	
2a. SECURITY CLASSIFICATION AUTHORITY		3. DISTRIBUTION / AVAILABILITY OF REPORT Approved for public release; distribution is unlimited.	
2b. DECLASSIFICATION / DOWNGRADING SCHEDULE		4. PERFORMING ORGANIZATION REPORT NUMBER(S) <b>WL-TR-92-4004</b>	
4. PERFORMING ORGANIZATION REPORT NUMBER(S) <b>WL-TR-92-4004</b>		5. MONITORING ORGANIZATION REPORT NUMBER(S)	
6a. NAME OF PERFORMING ORGANIZATION <b>Materials Lab, WL, AFSC</b>	6b. OFFICE SYMBOL (If applicable) <b>WL/MLBP</b>	7a. NAME OF MONITORING ORGANIZATION	
6c. ADDRESS (City, State, and ZIP Code) <b>Wright-Patterson AFB, OH 45433-6533</b>		7b. ADDRESS (City, State, and ZIP Code)	
8a. NAME OF FUNDING / SPONSORING ORGANIZATION	8b. OFFICE SYMBOL (If applicable)	9. PROCUREMENT INSTRUMENT IDENTIFICATION NUMBER	
8c. ADDRESS (City, State, and ZIP Code)		10. SOURCE OF FUNDING NUMBERS	
		PROGRAM ELEMENT NO. <b>61102F</b>	PROJECT NO. <b>2303</b>
		TASK NO. <b>Q3</b>	WORK UNIT ACCESSION NO. <b>07</b>
11. TITLE (Include Security Classification) <b>Characterization and Analysis of Defects in Nonlinear Optical Molecular Composite Films</b>			
12. PERSONAL AUTHOR(S) <b>Mehta and Charles Y-C Lee</b>			
13a. TYPE OF REPORT <b>Final</b>	13b. TIME COVERED FROM <b>Sep 89</b> TO <b>Apr 91</b>	14. DATE OF REPORT (Year, Month, Day) <b>1992 April</b>	15. PAGE COUNT <b>109</b>
16. SUPPLEMENTARY NOTATION			
17. COSATI CODES		18. SUBJECT TERMS (Continue on reverse if necessary and identify by block number)	
FIELD	GROUP	SUB-GROUP	
<b>07</b>	<b>04</b>		
<b>11</b>	<b>04</b>		
19. ABSTRACT (Continue on reverse if necessary and identify by block number) Recently in our laboratory, improved optical quality films of PBZT were fabricated by extruding low concentration solutions in methane sulphonic acid. The films, even though being extruded from an apparatus that was not designed for optical films, showed a dramatic improvement in the optical quality over those which were used in the previous measurements. X <sup>3</sup> measurements of these films also indicated that the x <sup>3</sup> values of these films were substantially higher than the previously reported values. However, the films were not of sufficient quality for wave-guiding experiments. This study was to identify the optical defects of the films so that the technique and the equipment can be improved to generate wave-guiding quality films with other NLO polymers. Two classes of defects have been identified and will be described in this report. The equipment modifications being implemented are documented.			
20. DISTRIBUTION / AVAILABILITY OF ABSTRACT <input checked="" type="checkbox"/> UNCLASSIFIED UNLIMITED <input type="checkbox"/> SAME AS RPT. <input type="checkbox"/> DTIC USERS		21. ABSTRACT SECURITY CLASSIFICATION <b>Unclassified</b>	
22a. NAME OF RESPONSIBLE INDIVIDUAL <b>Charles Y-C Lee</b>		22b. TELEPHONE (Include Area Code) <b>513-255-9155</b>	22c. OFFICE SYMBOL <b>WL/MLBP</b>

## FOREWORD

This report was prepared by the Polymer Branch, Nonmetallic Materials Division. The work was initiated under Project 2303, "Nonmetallic and Composite Materials," Task No. 2303Q3, Work Unit Directive 2303Q307, "Structural Resins." It was administered under the direction of the Materials Directorate, Wright Laboratory, Air Force Systems Command, Wright-Patterson Air Force Base, Ohio with Dr. Robert C. Evers as the Materials Directorate Project Scientist. Coauthors were Rajeev Mehta, Adtech Systems Research Inc., and Charles Y.-C. Lee, Materials Directorate (WL/MLBP). This report covers research conducted from September 1989 to April 1991.

## CONTENTS

Section	Page
1. INTRODUCTION	.....1
2. EXPERIMENTAL	.....3
3. RESULTS AND DISCUSSION	.....9
Processing parameters for film extrusion	.....9
Two classes of defects	...12
REFERENCES	...53
APPENDIX A	...57
APPENDIX A1	...64
APPENDIX A2	...68
APPENDIX A3	...88
APPENDIX B	...101

## FIGURES

Figure	Page
1. Schematic of Film Extrusion Apparatus.	.....5
2. Drying Configurations for the Wet Extruded Film.	.....6
3. Polymers Used for NLO Studies.	.....7
4. Photograph of a PBZT Ring Mounted Sample.	.....14
5. Scanning Electron Micrographs of Freeze Fractured Cross-Section of : (a) ZYTEL 330 and (b) 6F-PBO Films.	.....15
6. Optical Micrograph of a PBZT Film Showing Ellipsoidal Micro-Voids.	.....20
7. Scanning Electron Micrograph of a PBZT Film Showing Micro-Voids.	.....21
8. Axially Moving Plunger in a Cylinder.	.....28
9. Computed Streamlines in Front of an Advancing Plunger.	.....29
10. Optical Micrograph of a PBZT Film - Hand-Sheared and Coagulated in a 50/50 MSA/Water Non-Solvent.	.....37
11. Scanning Electron Micrograph of a PBZT Film - Hand-Sheared and Coagulated in a 50/50 MSA/Water Non-Solvent.	.....38
12. Processing Window Concept for Achieving Low Number -Density of Micro-Voids in the Slowly Coagulated Films.	.....39
13. Optical Micrograph of a PBZT/6F-PBO Film Showing a Macro-Void.	.....44
14. Optical Micrograph of a 6F-PBO Film Showing the Lines in the Transverse Direction.	.....47

## FIGURES (continued)

Figure	Page
15. Scanning Electron Micrograph of a 6F-PBO Film Showing Two Different Kinds of Lines in the Transverse Direction.	.....48
16. Scanning Electron Micrograph of a 6F-PBO Film Showing Lines in the Transverse Direction.	.....49
17. Optical Micrograph of a PBZT/6F-PBO Film Showing the Lines in the Machine Direction.	.....51
18. Scanning Electron Micrograph of PBZT/6F-PBO Film Showing the Lines in the Machine Direction.	.....52
A -1. 100X View of Standard Mott Porous Metal Filters.	.....59
A -2. Flow Characteristics of Mott Porous Metal Filters.	.....61

## TABLES

Table	Page
1. List of Film Extrusions and the Corresponding Initial Pressure Drops.	.....8
2. Casting Thickness vs. Micro-Void Content.	.....36
3. List of Experiments for Coagulation of 1% PBZT/MSA Solution in 50/50 MSA/Water Non-Solvent.	.....40
4. Classification Scheme for Micro-Voids.	.....43
A - 1. Pressure Drop for Mott Filters.	.....63
B - 1. Coagulation Rates for an Isotropic PBZT/MSA Solution in Various Non-Solvents (ref. 38).	....102

## SECTION 1

### INTRODUCTION

The high degree of delocalization of heterocyclic aromatic molecules makes this class of chemistry ideal for hyperpolarizability studies and NLO polymer development. The  $\chi^{(3)}$  value of a PBZT (poly (p-phenylene benzobisthiazole)) (1) film was characterized (2) in 1985. The result showed that the film had a relatively high  $\chi^{(3)}$  value and a very fast response time. Since then, much effort has been invested (3-6) in utilizing the conjugation in heterocyclic aromatic chemistry to enhance the third order non-linearity of polymeric materials. This class of polymers are relatively difficult to process into optical quality films or structures. This study is to use PBZT and similar molecules as model polymers for developing processing routes to form films for optical studies.

Spin Coating technique is the most commonly used technique for preparing NLO polymer films. This technique does not always work well for high molecular weight polymers and can only be used if the polymer is soluble in suitable solvents. Thus a lot of polymers, for example, the rigid rod PBZT, will be unsuitable for spin coating. Most of these polymers are unsuitable for other conventional thin film preparation techniques like Dip coating, Vacuum deposition and Sol-Gel processing. This fact renders the measurement of  $\chi^{(3)}$  of many polymers impossible because thin films with sufficient optical quality and transparency cannot be prepared.

Solutions of sufficiently high viscosity can be extruded through a die and the solvent can be removed through coagulation with a non-solvent to form thin films. This technique has been widely used for PBZT (7-9).  $\chi^{(3)}$  of a PBZT film extruded from polyphosphoric acid was measured (2) several years ago, and the result showed that PBZT had an unusually high  $\chi^{(3)}$  ( $1 \times 10^{-11}$  e.s.u.) and a very fast response time (500 femtoseconds). Recently in our laboratory, improved optical quality films of PBZT were fabricated by extruding low concentration solutions in methane sulphonic acid. The setup and the procedure were similar to that used for fabricating structural films (9). The films, even though being extruded from an apparatus that was not designed for optical films, showed a dramatic improvement in the optical quality over those which were used in the previous measurements.  $\chi^{(3)}$  measurements of these films (10) also indicated that the  $\chi^{(3)}$  values of these films were substantially higher than the previously reported values. However, the films were not of sufficient quality for wave-guiding experiments. For wave-guiding, optical loss must be minimized. There are two factors contributing to the optical loss: optical absorption and scattering due to defects (11). This study was to identify the optical defects of the films so that the technique and the equipment can be improved to generate wave-guiding quality films with other NLO polymers. Identifying these defects will also help in characterizing the specimens that were used for NLO measurements. Two classes of defects have been identified and will be described in the following sections. Modification and equipment upgrade are currently being implemented in an attempt to eliminate some of these defects.

## **SECTION 2**

### **EXPERIMENTAL**

The polymer solutions were prepared by mixing predetermined weight composition(s) of the polymer(s) in methane sulphonic acid (MSA) solvent at ambient temperature, until the solutions were deemed to be homogeneous by optical microscopy. Thin films were extruded in the film extrusion apparatus (Fig. 1). The film extrusion apparatus consists of (a) a pressurizing piston assembly, (b) a coat-hanger die, (c) a coagulation bath, and (d) a take-up mechanism. The coagulated films were washed in distilled water and kept in distilled water in a wet state until ready for mounting and drying. "Good" sections of films were selected for specimen mounting by visual inspection. Four drying configurations were used : (a) wet film mounted on a thin glass ring; wet film sandwiched under tension between (b) two microscopic slides, (c) one teflon coated microscopic slide and a plain slide, (d) teflon coated metal plate with a window and a plain slide (Fig. 2). The best quality specimens were selected and sent out for NLO measurements.

The characterization of defects in the film samples was done by standard optical microscopy and scanning electron microscopy. The instruments used were ORTHOLUX II POL - BK optical microscope and JEOL JSM - 840 scanning electron microscope.

Films were prepared from PBZT, 6F-PBO (12) (polybenzobisoxazole containing hexafluorinated moities), ZYTEL 330

(13) (an amorphous nylon, obtained commercially from E. I. DuPont Chemical Co.), LUBRIZOL (14) (poly (sodium 2-acryamido-22-methylpropanesulfonate)), LUBRIZOL Monomer (obtained commercially from Lubrizol Co.), ABPBT(9) (poly (2, 5(6') benzobisthiazole)) and PBT-Thiophene (5) (copolymer of PBZT and thiophene) (Fig. 3). The type of films studied can be divided into four categories and they are (1) 100% PBZT and 100% amorphous polymer films, (2) PBZT/amorphous polymer in 50:50 weight ratio, (3) PBZT/ZYTEL 330 in different weight ratios, and (4) 100% PBZT extruded from 1%, 2% and 3% solution. A complete list of extrusions along with their corresponding extrusion pressure drops (which were found to bear a linear relationship with the solution viscosities) is given in Table 1. The rationale for the above extrusions and for choosing the solid content in the respective extrusion solutions is discussed in Section 3.

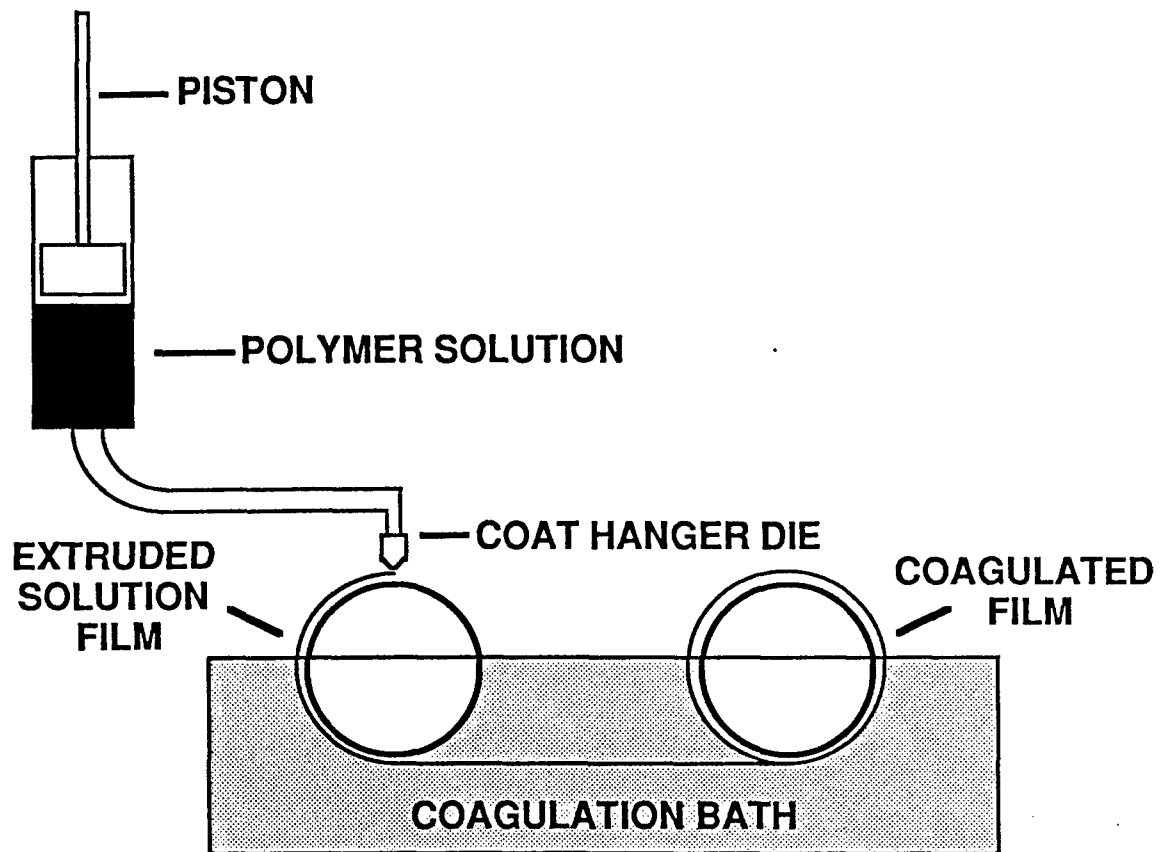
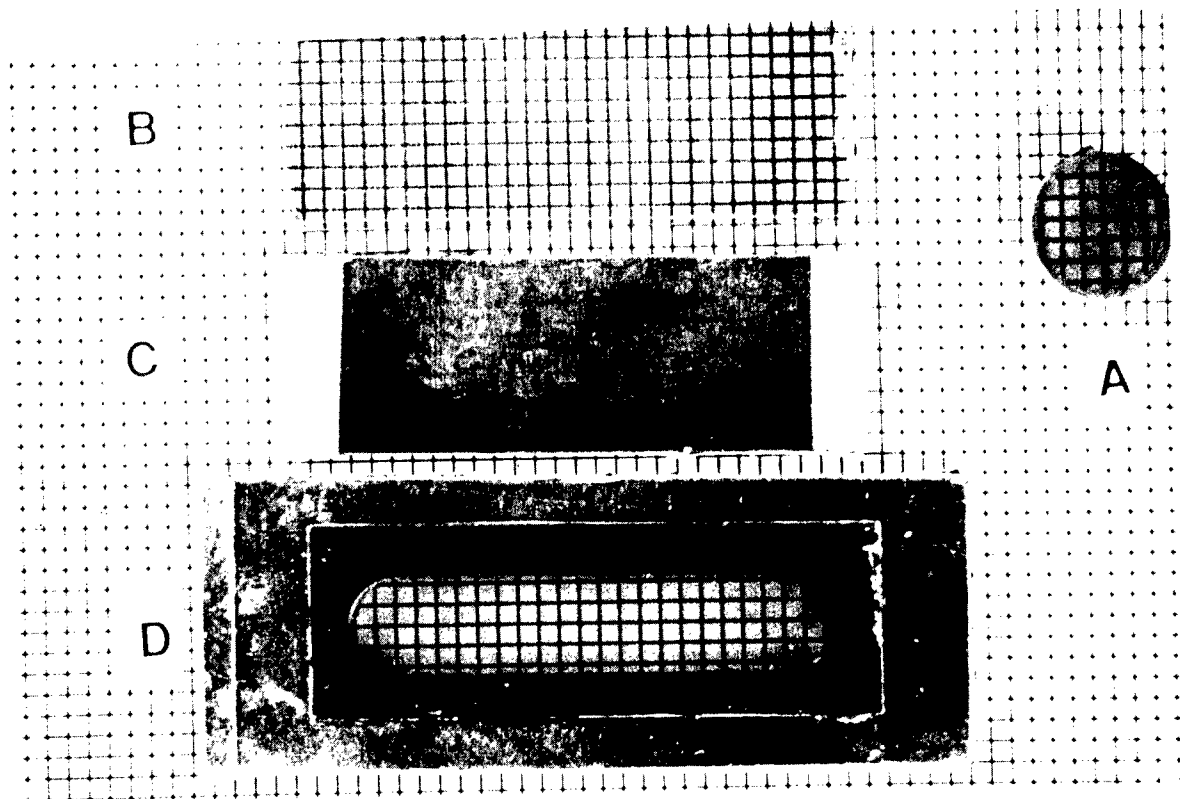


Figure 1. Schematic of Film Extrusion Apparatus.

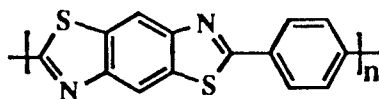


**Figure 2.** Drying Configurations for the Wet Extruded Film - (A) Wet Film Mounted on a Thin Glass Ring; Wet Film Sandwiched Under Tension Between - (B) Two Microscopic Slides, (C) One Teflon Coated Microscopic Slide and a Plain Slide, and (D) Teflon Coated Metal Plate With a Window and a Plain Slide.

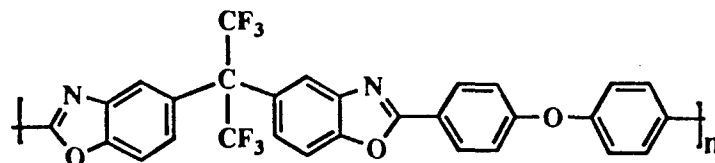
**POLYMER  
(Acronym)**

**CHEMICAL STRUCTURE**

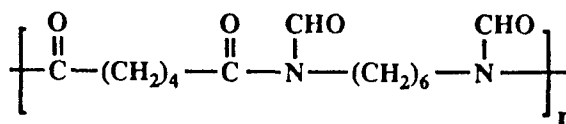
**PBZT**



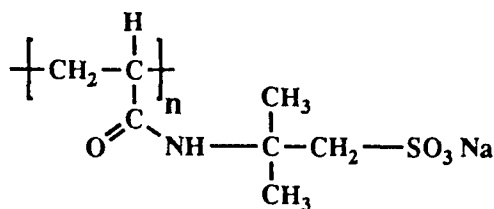
**6F-PBO**



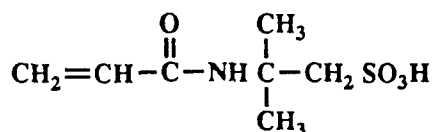
**ZYTEL 330**



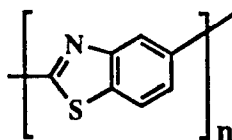
**LUBRIZOL**



**LUBRIZOL  
MONOMER**



**ABPBT**



**PBT-THIOPHENE**

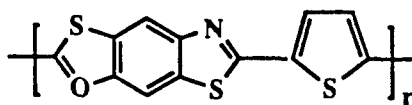


Figure 3. Polymers Used for NLO Studies.

Table 1. List of Film Extrusions and the Corresponding Initial Pressure Drops.

EXTRUSION SOLUTION	INITIAL PRESSURE DROP (PSI)
2% PBZT/6F-PBO (50/50)	45
1% PBZT	10
5% 6F-PBO	6
1% PBZT	10
2% PBZT/ZYTEL 330 (50/50)	40
3% PBZT/ZYTEL 330 (50/50)	60
1% PBZT	12
20% ZYTEL 330	30
1% PBZT	20
2% PBZT	45
3% PBZT/6F-PBO (50/50)	100
2.5% PBZT/LUBRIZOL (50/50)	50
2% PBZT/LUBRIZOL MONOMER (50/50)	8
2% PBZT	50
3% PBZT	200
2.5% PBZT/AB-PBT	40
6% ABPBT	100
1.87% PBZT/ZYTEL 330 (80/20)	50
4% PBZT-THIOPHENE	25
2% PBZT/PBZT-THIOPHENE (50/50)	15
3.75% PBZT/ZYTEL 330 (40/60)	30
3.5% PBZT/ZYTEL 330 (20/80)	7

## SECTION 3

### RESULTS AND DISCUSSION

#### PROCESSING PARAMETERS FOR FILM EXTRUSION

##### Elasticity of the solution

The success of the film extrusion process is contingent upon the 'film forming' characteristics of the solution. Since no carrier tape is used in the film extrusion operation, the polymer solution should have the requisite elasticity to form a film. Qualitatively, the entanglements of the polymer chains give the solution integrity, i.e., processability with regard to product formation (film). For the flexible polymers, the elasticity of the solution is related to the ratio of the molecular weight between entanglements and the weight average molecular weight (9). In general, the solution elasticity would be related to the bulk viscosity. In other words, there exists a lower limit for the viscosity (a function of molecular weight of the polymer and solid content of the solution) of the solution for film extrusion. Thus, whereas a PBZT film could be extruded from a 1% PBZT/MSA solution, successful extrusion of a ZYTEL 330 (a low molecular weight condensation polymer) film required a 20% Zytel 330/MSA solution. An attempt to obtain a ZYTEL 330 film from a 10% Zytel 330 solution was unsuccessful due to the disintegration of the film after coagulation (15).

### Isotropic nature of the solution

A necessary but not sufficient condition for obtaining a transparent film through the coagulation process is that the polymer solution should be transparent. In other words, it is essential that there should not be many light scattering entities present in the solution. In the case of rigid-rod polymers and their composites, the solution must be below the critical concentration (critical concentration,  $C_{cr}$ , is the concentration at which the isotropic to anisotropic + isotropic phase transition occurs). According to the Flory's "athermal" theory (16), the dominant factors affecting the critical concentration are the aspect ratio of the rigid molecules and the composition ratio of rigid polymer and coil polymer (in a ternary system). The PBZT used in this study had an intrinsic viscosity of 16 dl/gm. The PBZT/MSA system ( PBZT IV = 16 dl/gm ) has a critical concentration of 3.6% (17), above which the nematic liquid crystal domains would form. The liquid crystalline character of the solution would be preserved through fast coagulation and the domain boundaries in the coagulated film would serve as scatterers of light. The critical concentration for a 50/50 PBZT/ZYTEL 330 system is reported to be 4.8% (16). All the extrusion solutions in this study were optically transparent, though not colorless.

### Equipment constraints

Even when the solution is transparent and have the requisite elasticity, it must satisfy some other conditions imposed by the equipment constraints. For example, the extrusion viscosity should be low enough so that the maximum pressure drop in the system is

below 250 lb<sub>f</sub>/in.<sup>2</sup>. This is due to two reasons : (1) the transducer which is employed to monitor the pressure in the extrusion cylinder is rated for a maximum of 250 lb<sub>f</sub>/in.<sup>2</sup>, and (2) the sealing afforded by the teflon pieces in the extrusion cylinder (which are used to prevent the corrosion of the cylinder) may not be good above a pressure of 250 lb<sub>f</sub>/in.<sup>2</sup>. Another equipment constraint on the viscosity of the extrusion solution is due to the configuration of the casting die and the casting roller. Since the die is placed vertically on top of the roller in the 'doctor-blade' arrangement (the gap between the casting die and the roller is much smaller than the die opening), there exists an upper and lower limit, outside of which the film extrusion operation would not be successful. Qualitatively, these limits are higher and lower, respectively, than the viscosity of the solutions used in this study.

#### Shrinkage of the film during coagulation

When the film solution is coagulated, it necks down so that the width of the coagulated wet film is less than the width of the casting die. According to Hecht (18), the degree of necking down depends principally on the polymer solution/melt, the draw ratio, and the distance between the die lip and the point where the film solution is coagulated. The draw ratio, in all extrusion runs, was kept close to unity (because of the low tensile strength of the wet film). Also, it is difficult to significantly change the distance between the die lip and the coagulation front. However, a correlating between the shrinkage and the viscosity of the extrusion solution was observed. If the solution viscosity is above a certain value (approximately 1500 Poise

at  $10 \text{ s}^{-1}$ ), the amount of shrinkage decreases dramatically. No attempt was made to find an explanation for this correlation.

Additionally, neck-in is also related to an entirely different phenomenon which apparently does not depend on the viscosity of the polymer solution. If the die is used in the configuration which has been described in the sub-section above, there is an entrapment of an air layer between the film solution and the drum. The air layer causes an uneven neck-in among other film quality problems. This air layer has been reported to be eliminated (and thereby ensuring satisfactory film solution adherence to the casting drum) by various methods (reviewed in ref. 18) - heating the drum, pinning the edges of the film solution with air jets, using a contact roll or an air knife, and vacuum suction. We found that the air layer can be eliminated (and the neck-in significantly reduced) if a bulge of extrusion solution is maintained on the casting roller behind the die relative to the extrusion direction. We should mention that it is easy to maintain a steady bulge because the typical extrusion speed employed is very slow.

## TWO CLASSES OF DEFECTS

Polymer film samples can be used for either  $\chi^{(3)}$  determination experiments or wave-guiding experiments. The  $\chi^{(3)}$  measurement experiments are more forgiving with respect to the maximum tolerable optical loss. For example, PBZT and PBZT/ZYTEL 330 films are amenable to  $\chi^{(3)}$  measurement experiments but the optical quality is insufficient for wave-guiding experiments. On the other

hand, optical losses in pure ZYTEL 330 and pure 6F-PBO films are high enough to render their  $\chi^{(3)}$  determination impossible. Analysis of the film samples revealed that there exists two distinct classes of scattering processes. The defects have been arbitrarily classified into two categories - "defects of higher order" and "defects of lower order". The "defects of higher order" are the defects which render the film with very poor optical quality so that  $\chi^{(3)}$  measurements can not be reliably conducted. The "defects of lower order" are found in films that are of sufficiently good optical quality (Fig. 4) for  $\chi^{(3)}$  measurement, but not good enough for wave-guiding. The origin, characteristics and the steps taken towards their elimination are discussed in the following sections.

### Defects of higher order

As mentioned above, pure ZYTEL 330 and pure 6F-PBO films have very large optical losses. The color of the ZYTEL 330 film is opaque white and the 6F-PBO film is translucent white. The SEM micrographs of the freeze fractured (in liquid nitrogen) cross-sections of these films are shown in Fig. 5. The scattering due to the irregular voids in these films clearly leads to the high optical losses. We should mention that at the same magnification, the corresponding micrographs of the PBZT and PBZT/ZYTEL 330 films appear as non-porous surfaces. The extrusion solution was clear on the casting drum until it hit the water bath. Transformation of a colorless transparent solution into an opaque or translucent film which is

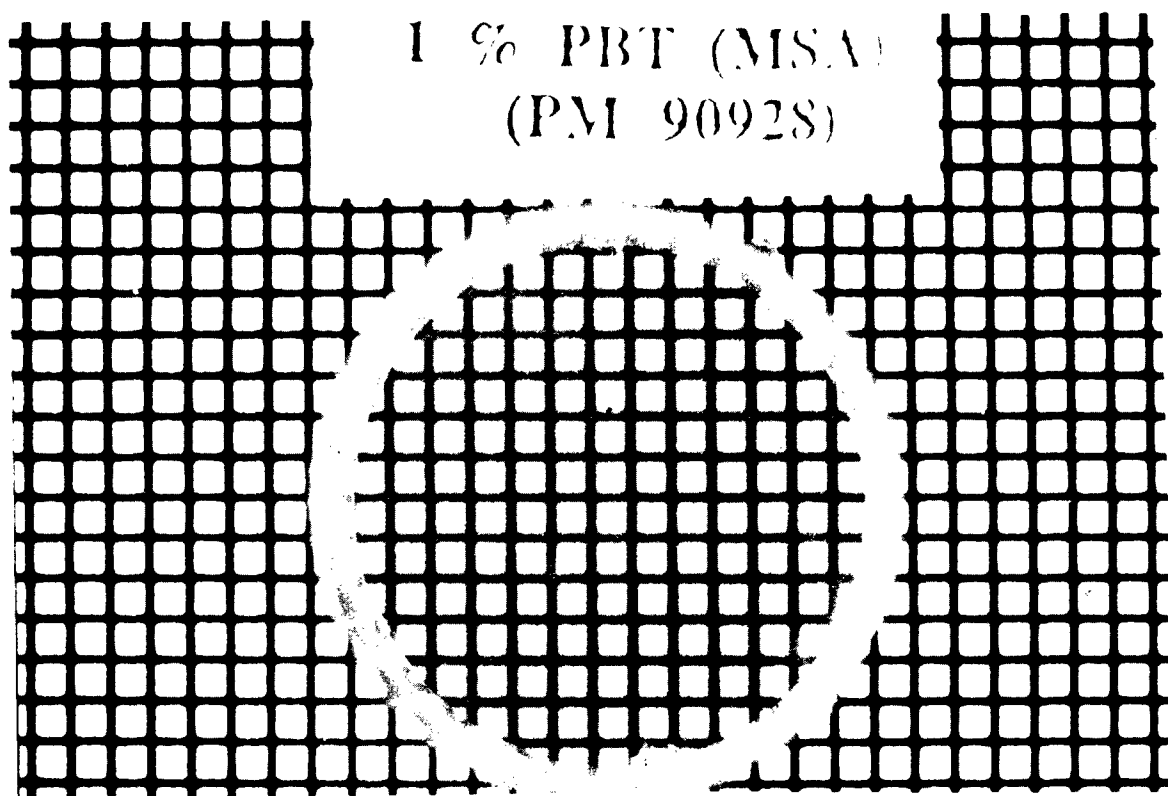


**Figure 4.** Photograph of a PBZT Ring Mounted Sample.

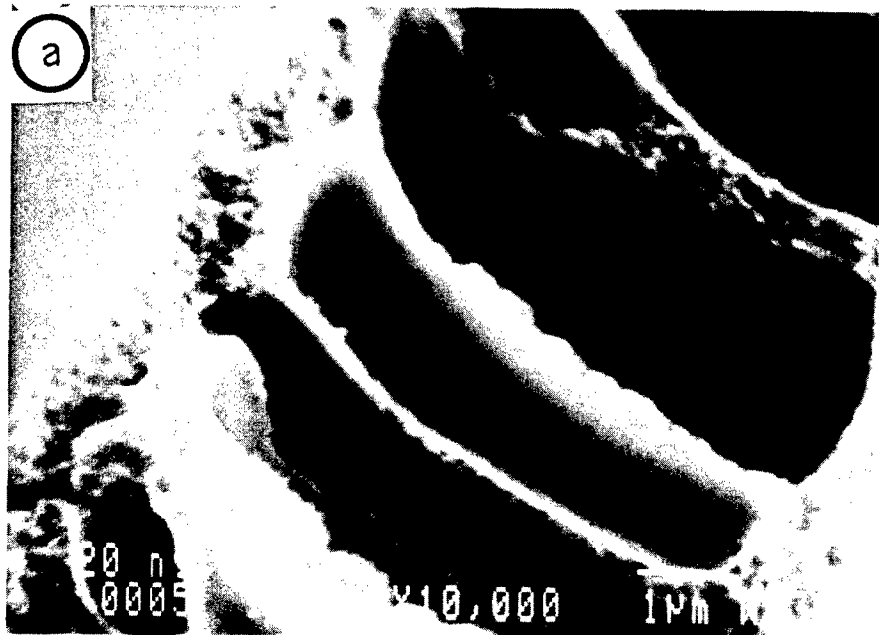


Figure 5. Scanning Electron Micrographs of Freeze Fractured Cross-Section of : (a) ZYTEL 330, and (b) 6F-PBO Films.

characterized by an irregular void morphology, is clearly related to the coagulation process.

A comprehensive treatment of the solidification process in a polymer-solvent(s)-non-solvent(s) system has been given by Ziabicki (19). The homogeneity of the coagulated structure depends on the phase equilibria in polymer - solvent - non-solvent system and the mass transfer route (defined by the ratio of the outward flux of solvent,  $j_s$ , to the inward flux of non-solvent,  $j_n$ ). In general, the coagulation conditions where the ratio,  $j_s/j_n$ , is high and phase separation is avoided yields the most dense and homogeneous structure.

When we translate this for the coagulation process of pure ZYTEL 330 and pure 6F-PBO, the following picture emerges. The outward flux of the solvent is low compared to the inward flux of the non-solvent. Thus, by the time enough MSA solvent has diffused out of the polymer solution to cause its solidification, too much water must have diffused into the film during coagulation. The water aggregates in pockets forming the light scattering voids. In view of this picture, coagulation of ZYTEL 330 and 6F-PBO was carried out in non-solvents with greater 'coagulation power' than water. We should remark that decreasing the coagulation time is not necessarily analogous to increasing the  $j_s/j_n$  ratio. However, in order to strictly satisfy the latter criterion, it would require a detailed study for every single non-solvent.

The 20% ZYTEL 330/MSA and 5% 6F-PBO/MSA solutions, casted on a microscopic slide, were coagulated in non-solvents with higher 'coagulation power' than water at room temperature - water at 60 °C,

triethylamine, tetrahydrofuran (THF), and solutions of KOH and NaOH of different strengths. In addition to these polymer solutions, the 15% ZYTEL 330/MSA and 15% ZYTEL 330/Sulphuric Acid solutions were also studied. Only the ZYTEL 330 film obtained from coagulation in THF showed a slight improvement in the optical clarity as compared to the corresponding film coagulated in water. Since pure Zytel 330 and pure 6F-PBO films are not expected to have significant  $\chi^{(3)}$  values (these polymers were being studied to evaluate their potential to act as processing aids for putting molecules with high values of second order hyperpolarizabilities into high optical quality products), subsequent attention was focussed on other flexible polymers and the efforts towards eliminating the 'defects of higher order' in ZYTEL 330 and 6F-PBO were suspended.

### **Defects of lower order**

Analysis of the films, which have sufficient optical clarity to permit their  $\chi^{(3)}$  determination but fail to wave-guide, revealed the presence of five different defects. These are:

1. Micro-voids,
2. Macro-voids,
3. Particles,
4. Lines in the transverse direction,
5. Lines in the machine direction.

These defects are discussed in the following sections. We should, however, mention that it is unclear if these defects alone are responsible for rendering these films unsuitable for wave-guiding.

## Micro-voids

### Characterization

The micro-voids are about 20-25 microns in size, though smaller micro-voids are also present (Fig. 6). In general, they are ellipsoidal in shape with their long axis oriented mostly along the machine direction. The only exception is the 5% 6F-PBO (the lowest viscosity dope) samples, where they are mainly spherical in shape. Also, interestingly, a solid particle is present in each micro-void (Fig. 6), though in some cases multiple dots are also observed. With the exception of 1% PBZT sample (Fig. 7), these micro-voids were observable under an optical microscope but were not observable in SEM (in secondary electron imaging mode) in the ring mounted samples. Since the 1% PBZT film is thinner than other films (1 micron vs other films which are 2-10 microns thick), it would appear that these micro-voids are internal and not surface holes.

### Origin

For analyzing the origin of the micro-voids, the film processing was divided into five steps:

Step a : stirring the polymer and the solvent (distilled MSA) under nitrogen,

Step b : transfer of dope from the reactor vessel to the extrusion cylinder,

Step c : deaeration of the dope,

Step d : removal of air present between the extrusion piston and the dope (pre-extrusion),

Step e : coagulation of the dope in the water bath.

Analysis of the first four steps addresses the theory that micro-voids in the films are a result of gas bubbles present in the extrusion solution. The diffusion of air in the dope can be considered as an 'unsteady state diffusion in a semi-infinite geometry' problem. In such a problem (20), the following variable can be used to estimate how far or how long the mass transfer has occurred:

$$(\text{length})^2 / (\text{diffusion coefficient}) (\text{time})$$

This variable is the argument of the error function of the semi-infinite slab and is central to the time dependence of the diffusion. Basically, the process is significantly advanced when this variable equals unity. Using the typical value for diffusion coefficient of air in liquids, it can be easily shown that it will take about 30 days for the air to penetrate 0.1 cm of dope. Clearly, air cannot get into the dope to a significant extent by the process of simple diffusion.

#### Steps a and b

The air can get into the dope during step (a) by entrainment and mechanical disintegration (21). Gas can be entrained into the liquid by the surface ripples or waves, and by the vortical swirl of a mass of agitated liquid about the axis of a rotating agitator. Small bubbles probably form near the surface of the liquid and are caught into the path of eddies whose velocity exceeds the terminal

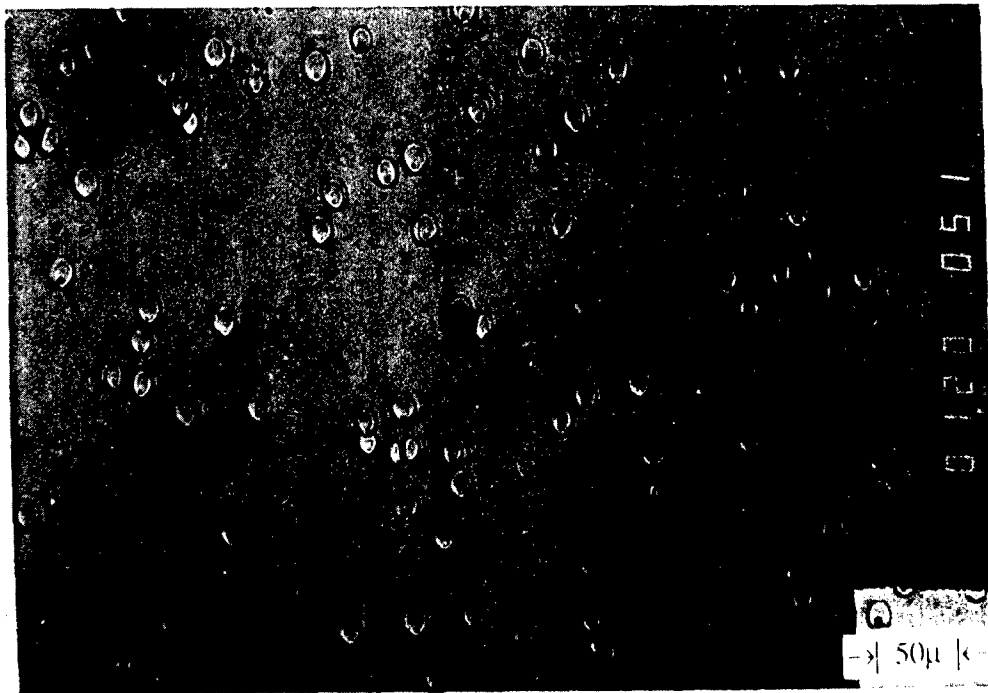


**Figure 6.** Optical Micrograph of a PBZT Film Showing Ellipsoidal Micro-Voids.

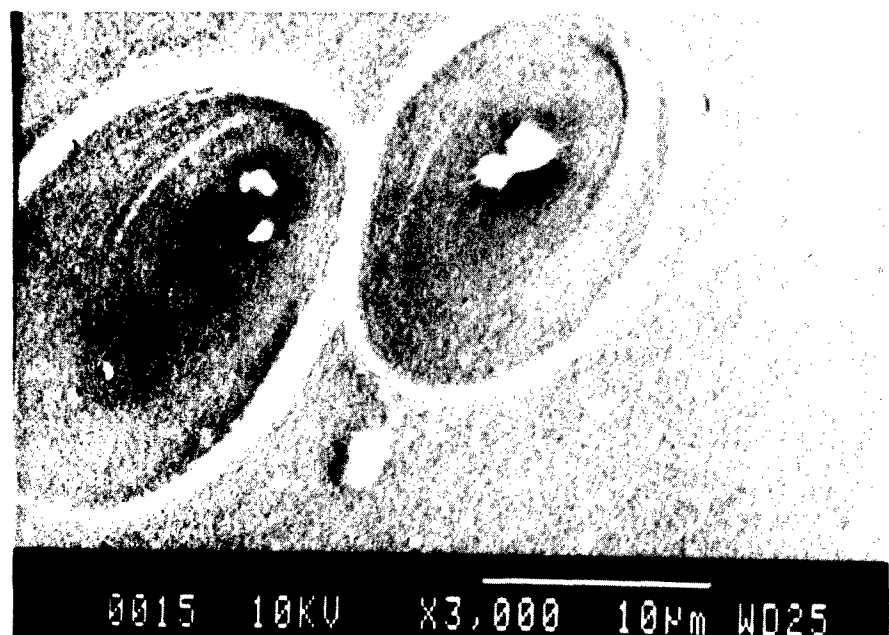


**Figure 7. Scanning Electron Micrograph of a PBZT Film Showing Micro-Voids.**

velocity of the bubbles. The disintegration of a submerged mass of gas takes place by the turbulent tearing of smaller bubbles away from the exterior of the larger mass or by the influx of surface tension or shear forces into a cylindrical or disc form.

### Steps a and b

The air can get into the dope during step (a) by entrainment and mechanical disintegration (21). Gas can be entrained into the liquid by the surface ripples or waves, and by the vortical swirl of a mass of agitated liquid about the axis of a rotating agitator. Small bubbles probably form near the surface of the liquid and are caught into the path of eddies whose velocity exceeds the terminal velocity of the bubbles. The disintegration of a submerged mass of gas takes place by the turbulent tearing of smaller bubbles away from the exterior of the larger mass or by the influx of surface tension or shear forces into a cylindrical or disc form. A fluid cylinder that is greater in length than in circumference is unstable and tends to break spontaneously into two or more spheres. These effects account for the action of fluid attrition and of an agitator in the disintegration of the suspended air. However, the entrapment and disintegration of gas in step (a) and entrapment of air in step (b) are not practically calculable (21).

The first logical step towards eliminating bubbles from the dopes was to prevent the air entrapment. Thus, the dope (1 wt% PBZT/MSA) was stirred under vacuum and then transferred in a vacuum oven using an ingenious setup. The number density and the size of micro-voids in the extruded film were the same as in the 1 wt% PBZT/MSA film extruded with steps (a) and (b) unchanged.

Clearly the problem lay somewhere else. Additionally, since a moving part (stirrer) is present during mixing of the dope, a good vacuum can not be attained. This in turn exposes the dope to moisture in the air (albeit at low pressure) for long periods of time. Thus, stirring of the dope under dry nitrogen was resumed.

### Step c

The next effort was towards understanding the deaeration process (step c) and to determine if the deaeration time of about 14 hrs., which is typically used, was sufficient. The dope after being transferred to the extrusion cylinder (step b) contains bubbles and the dissolved air. Even though there is no quantitative theory about the formation of bubbles from the dissolved air, it is understood that the bubble formation from the dissolved gas can take place only by desupersaturation (22). Thus, the dissolved air at atmospheric pressure cannot lead to bubbles in the film. In other words, undissolved air must be present in the dope at room temperature and pressure to result in bubbles in film.

### Calculation of the deaeration time

Unstable suspensions of bubbles in the fluid are separated by the action of buoyant force on the bubbles, a special case of gravity settling. The upward velocity of a sphere in a medium can be approximately calculated by Stokes's law (23), and is given by eq. (1) (23):

$$u_t = g D_p^2 (\rho_p - \rho) / (18\mu) \quad (1)$$

where,  
 $u_t$  - terminal settling velocity of the sphere,  
 $D_p^2$  - diameter of the sphere,  
 $\rho_p$  - density of the sphere,  
 $\rho$  - density of the medium,  
 $\mu$  - viscosity of the medium

Application of vacuum helps to hasten the deaeration process by virtue of increased bubble size. Since the micro-void size in the film is about 20 microns, the size of bubbles under vacuum can be estimated. Assuming a conservative value for vacuum of 29 in.Hg., the diameter of bubbles in the dope would be about 600 microns. Substituting this value in the above expression, the following expression can be easily derived. The terminal velocity,  $u_t$ , is given by eq. (2) :

$$u_t = 458 / \text{Viscosity (poise) inch/hr} \quad (2)$$

This expression has been derived by assuming that the bubble size in the dope at atmospheric pressure is equal to the size of the micro-voids in the dried film. This is probably incorrect and the the actual size of the bubbles in the extrusion solution at atmospheric pressure might be much larger than 20 microns. Thus, the optimum deaeration time would be lower than the calculated value. Using the above expression- for about 1 inch (height) of the dope (1 wt%

PBZT/MSA - viscosity at shear rate of 1 (1/s) = 550 poise) in the cylinder, all the bubbles should rise to the surface in less than 2 hours. In the case of 20% ZYTEL 330 (higher viscosity than 1% PBZT/MSA), the solution is transparent enough to permit a visual monitoring of the deaeration process. It was observed that on application of vacuum, bubbles, which are formed spontaneously, start rising towards the surface. In about 2 hours, the solution was completely free of all the bubbles. Also, the size of the bubbles in the dope during deaeration was in the 50-100 microns range.

For bubbles larger than 100 microns, the viscosity dependence predicted by Stokes's law in a highly viscous fluid is erroneous but the error is less than 15% (23). A more serious error results from the assumption in the Stokes's law which applies to rigid spheres. It is known that the circulation within the bubbles causes notable increase in its terminal velocity in the range of 100 microns to 1 mm, and flattening of bubbles 10 mm and larger appreciably decreases their velocity (23). In the latter size range, however, the velocity of rise is so high as to make deaeration a trivial problem. Thus, the values calculated from Stokes's law may be accepted as conservative value. Lastly, Stokes's law does not take into account the shear thinning of the fluid. The shear rate at the bubble wall (and the viscosity) is determined by the bubble's terminal velocity which in turn can be calculated after the viscosity is known. This problem has been solved for a power-law fluid (24). Thus care should be taken to use the correct viscosity in the Stokes's law. In our case, typically, the shear rates experienced by the fluid near the rising bubble would correspond to the zero shear rate viscosity of the polymer.

The mechanism by which the bubbles disappear after they have reached the top fluid layer is controversial. However, it is known that greater the viscosity, greater is the corresponding life of the bubbles at the surface. In fact, after the overnight deaeration of viscous dopes likes 3% PBZT/ZYTEL 330 (viscosity at 1/s shear rate = 5221 poise), some bubbles can be seen on the surface of the dope. In the case of the dopes, where bubbles were observed on the surface after an overnight deaeration, some solution was skimmed off the surface and the deaeration process was resumed. The skimming was repeated (after 2-3 hrs.) until no bubbles could be observed on the surface (typically, 2-3 times). Even though the deaeration time of 14 to 48 hours seems to be sufficient for deaeration, an attempt was made to increasing the efficiency of the deaeration process.

In the third experiment towards eliminating micro-voids from the films, the dope was transferred from the reactor vessel to a separator funnel. The subsequent slow transfer of the dope from the separator funnel into the extrusion cylinder through a 70 mils (1 mil = 25.4 microns) opening, under vacuum, was expected to accelerate the deaeration process. However, no difference could be observed in the number density of the micro-voids in the film which was subsequently extruded.

#### Step d

Lastly, the attention was focussed on the step (d), i.e. using the bleed valve on the piston to remove the trapped air between the dope and the extrusion piston when the latter is being lowered in the extrusion cylinder. Figures 8 and 9 show the extrusion cylinder

assembly and the computed velocity profile in the dope in the absence of air, respectively (25). Qualitatively, as the piston moves forward, the dope must acquire an inward radial velocity (in order to extrude from the opening in the cylinder), while gradually decelerating to a zero axial velocity. As the fluid continues to move inward, it acquires a positive axial velocity. Hence the result is an annular 'skin' of liquid moving toward the plunger and an inner 'core' moving away from it. Such a flow is commonly known as reverse 'fountain flow'. If a second fluid (air) is present along with the first (dope), the velocity profile would be altered but the circulatory motion (reverse fountain flow) would still be present. Thus if there is any air left between the piston and the plunger before extrusion, it will distribute itself throughout the dope.

Next, an estimate was made of the amount of air in the film from the optical micrographs. The volume fraction of air in the most films is of the order of 0.6% (assuming the thickness of the micro-voids is equal to the thickness of the dried film). This would mean that even if about  $0.098 \text{ cm}^3$  (height in the extrusion cylinder) of air is present between  $125 \text{ cm}^3$  of dope (assumed to be containing an equilibrium amount of dissolved air at room temperature and pressure) and the piston, it would be sufficient to result in the observed micro-voids in the film (that is assuming that bubbles in the solution result in micro-voids in the dried film). The 'bleeding button' on the piston is not adequate for removing the air to such an extent. Hence, a vacuum fitting was attached to the piston so that the trapped air can be almost entirely taken out. However, no difference in the number of micro-voids was observed in the films

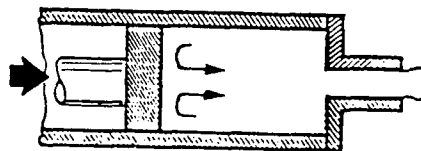


Figure 8. Axially Moving Plunger in a Cylinder.

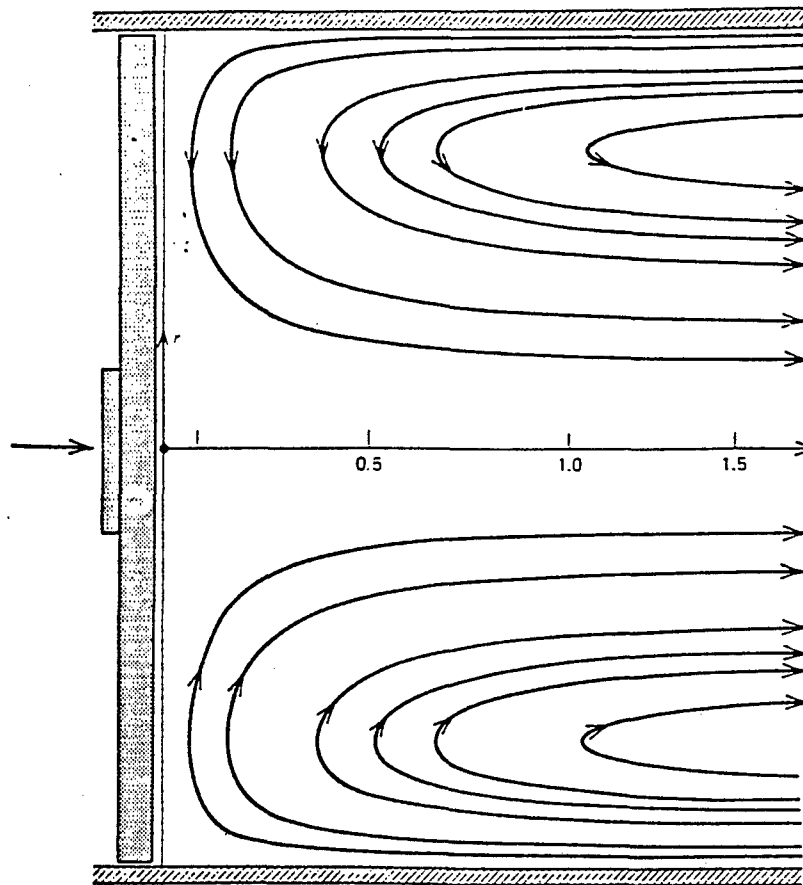


Figure 9. Computed Streamlines in Front of an Advancing Plunger.

which were subsequently extruded.

Thus, after a detailed analysis of the four steps, it was seemed unlikely that undissolved air in the dope leads to micro-voids in the coagulated films. It appeared that understanding the coagulation process (step e) held the key for solving the micro-void problem.

### Step e

It has been reported that micro-void formation can be suppressed by an application of other precipitation agents (usually with lower 'coagulation power'), an increase in the solvent content of the coagulation bath, lowering of the coagulation bath temperature or by gelation of the polymer solution (19, 26-39). The effect of gelation of the dope, temperature and solvent content of the coagulation bath, and the casting thickness and deaeration of dope on the micro-void content was studied by casting the solution on the microscopic slides. The advantage of producing hand-cast films over the extruded films is the tremendous saving in time and manpower. During the early part of the study, the films were produced by casting the dope on a clean microscopic slide and using a Teflon spacer to gauge the thickness. At a later stage, the coating of the dope on the microscopic slide was done by a doctor blade calibrated to the desired thickness. These slides were then immediately transferred to the coagulation bath. The coagulated slides were examined under the optical microscope.

### Effect of casting thickness on micro-voids

Two slides with vastly different casting dope thickness (not quantified) were coagulated in pure water at room temperature. The optical microscope examination of the dried films revealed that the size of the voids in the thin film was significantly less compared to the thick film. Thus the size of the micro-voids seemed to depend on the casting thickness of the dope. In the subsequent experiments the casting thickness was therefore kept constant. At a later stage during the course of this study, an old microtoming unit which had been converted into a sensitive and a stable 'doctro-blading' set up, was available. Using this set up, very thin films were prepared and the micro-void content was quantified. Table 2 lists these results. Since it is difficult to ascertain the accuracy of the casting thickness for '0.8 micron casting thickness' experiment, no inference should be drawn from these results about the specific relationship between the decrease in the casting thickness and the corresponding decrease in the micro-void size. However, it is clear that micro-void size decreases with the decrease in the casting thickness, though the micro-voids do not disappear in the films casted from extremely small casting thickness.

The casting thickness in the film extrusion operation is limited by the vertical play between the casting drum and the die and is typically between 1-2 mils. Thus, in the next set of experiments, a casting thickness of 2 mils was used. It was subsequently realized that due to the low transparency of the films, micro-void identification under the OM becomes difficult. Hence, at a later stage, a casting thickness of 1 mil was used.

#### Effect of different non-solvents on micro-voids

A quantitative study of the coagulation rates for the PBZT/MSA system and different non-solvents with lower coagulation power than water has been done by Berry, et al. (38). The selection of most of the non-solvents used in the present study was based on this study. The slides coated with 1% PBZT/MSA solution, at room temperature, were coagulated in various non-solvents. The coagulants studied were : 10-20-30-40-50-60 and 80% MSA/WATER, 30& 40% MSA/METHANOL, Triethylamine, Benzyl alcohol and Glycerol. The rate of coagulation of PBZT/MSA in all these non-solvents is lower than that in pure water (Appendix B).

a. It was observed that there was a substantial reduction in the micro-void number density when the non-solvent was 50-80% MSA/Water, 30-40% MSA/Methanol, Benzyl alcohol or Glycerol. In the case of Glycerol and benzyl alcohol only a few voids could be observed over the entire slide surface ( $3 \text{ in}^2$ ).

b. The optical quality of the films, however, was bad compared to the film obtained from coagulation in pure water. In all cases (except water at room temperature), a grainy net like structure was observed when the films were examined under the optical microscope (Fig. 10). Clearly, even though the number of voids had been reduced, the optical quality of the films had worsened because of a much greater number of these new features, which would be an efficient scatterers of visible light.

In order to investigate if these net like features are a result of some unknown glass substrate-dope- non-solvent interaction, a film extrusion was done in a 50% MSA/Water bath at  $8 \text{ }^\circ\text{C}$  . However, unlike the regular film extrusion where the dope is pumped through

a cylinder into a die, some dope was placed on the casting drum behind the die (relative to the extrusion direction) and the film was extruded using the die as a doctor blade. Expectedly, it was extremely difficult to detach the film from the casting drum (because of the lower coagulation rate) even when the speed of the drum was reduced significantly. The OM of the samples prepared from the film after immersing in pure water to remove the remaining acid, showed similar net like structure and a significant reduction in the void content. In addition to the non-solvents used in the PBZT/MSA study, the following non-solvents which were expected to have a greater 'coagulation power' than water, were also used : triethylamine, 20 N NaOH and THF (tetrahydrofuran). Again, micro-void reduction was observed with non-solvents with lower 'coagulation power'. An interesting observation was that the reduction in coagulation rate required to reduce the micro-void content always results in a net-like structure (50-60% MSA/Water, benzyl alcohol and glycerol). For the non-solvents which slightly higher coagulation rate (10-40% MSA/Water and 30-40% MSA/Methanol) neither any micro-void reduction nor any net-like structure was observed. In the case of triethylamine, 20N NaOH and THF, the film quality was bad because of the presence of cracks and different kinds of structures. Thus, the coagulation study of ABPBT/MSA system showed that the cause for net-like structure is not LC domain formation due to slower quenching. It would be pertinent to mention here that a vacuum casted (at 65 °C for 1 week) PBZT-Thiophene film (prepared by a fellow researcher) also showed the net-like structure when examined in the OM by us. The optical

losses in this vacuum casted film were high enough to render its  $\chi(3)$  determination impossible. Thus, it is possible that the origin of the net-like structure in the slowly coagulated film might be related to the high rigidity of the aromatic heterocyclic molecules.

The above results indicate that we were unable to identify the coagulation conditions (choice of a suitable non-solvent) where a significant reduction in the micro-void content can be achieved without the presence of the net-like structure. Next, an effort was made to locate a processing window wherein the micro-voids are formed (in low number density) before the formation of the net-like structure (a totally unacceptable feature) and where it might be possible to arrest/modify the coagulation process in the interim time interval (Fig. 12). 1% PBZT/MSA dope was coagulated in 50% and also in 60% MSA/Water bath for varying amounts of time (5 seconds to 24 hours) before being transferred to the water bath. Also, the coagulation history was varied from a slow to fast coagulation rate and vice versa. A typical list of experiments (for 50% MSA/Water) is shown in Table 3. No processing window could be found. The grainy net like structure clearly forms in less than 5 seconds. For a 1 mil casting thickness the coagulation time can be calculated from the coagulation rates available from ref. 38. The coagulation time is of the order of 3 seconds.

#### Effect of dope temperature and physical gelation on micro-voids

The temperature of the PBZT/MSA dope was lowered down to 8 °C and -8 °C. Both of these were then coagulated in water at 23 °C. In the latter case the dope's elastic modulus was too high (physical

gelation) for the doctor blade technique. So the dope was cooled down to  $-8^{\circ}\text{C}$  in a bottle and the bottle was immersed in water at  $23^{\circ}\text{C}$  for several days. The  $8^{\circ}\text{C}$  dope-film showed no difference from the  $23^{\circ}\text{C}$  dope-film. The  $-8^{\circ}\text{C}$  dope-coagulated block, however, showed the same net like structure when different sections were sliced from the dried block and examined under the OM. Thus, even when the non-solvent is water, reduction in micro-void content accompanied by the presence of a net-like structure is possible by a lowering of the coagulation rate.

#### Effect of water temperature on micro-voids

Only a single data point was studied. The temperature of the water (non-solvent) was decreased to  $3^{\circ}\text{C}$ . No change was observed in the micro-void content in the coagulated film from  $3^{\circ}\text{C}$  water as compared to the film coagulated from water at  $23^{\circ}\text{C}$ .

#### Effect of deaeration of the dope on micro-voids

Films prepared from undeaerated PBZT/MSA solution showed no difference in the micro-void content as compared to the films prepared from deaerated solutions.

#### Conclusion of the micro-void study

Micro-voids were identified as one of the scattering defects in the coagulated films. The micro-void content can be significantly reduced by decreasing the coagulation rate. However, a reduction in the micro-void content is always accompanied by an evolution of a 'net-like' structure, which is more efficient scatterer of light than the

**Table 2. Casting Thickness vs. Micro-Void Content**

<b>Casting Thickness (microns)</b>	<b>Micro-void size (microns)</b>	<b>Number of Micro-voids (in 0.5 sq mm)</b>
25	40	10-20
12	<20	20-40
0.8	<10	<10

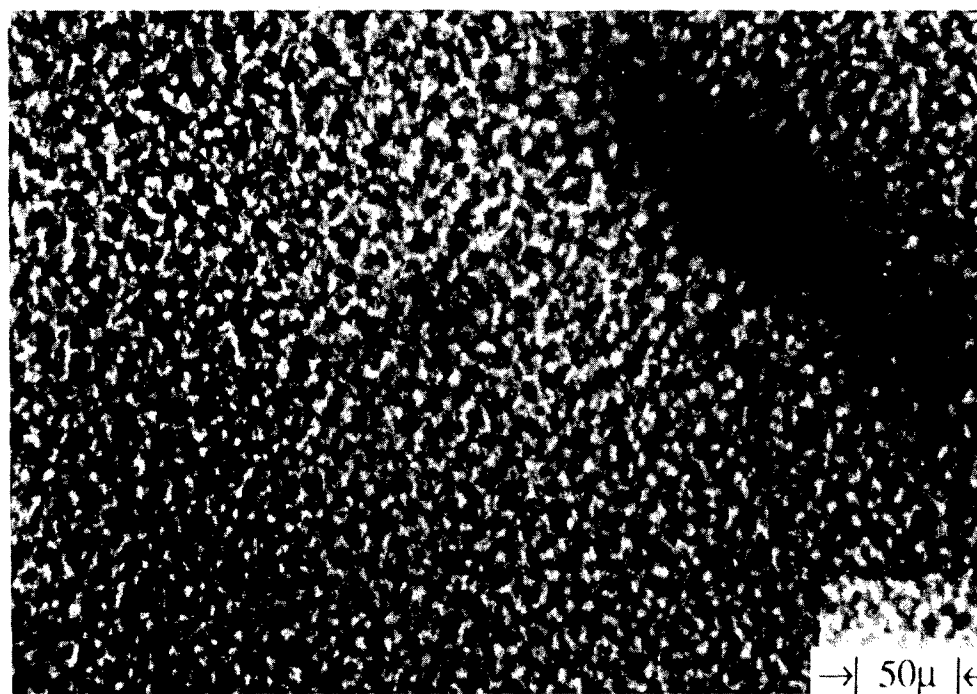


**Figure 10.** Optical Micrograph of a PBZT Film - Hand Sheared and Coagulated in a 50/50 MSA/Water Non-Solvent.

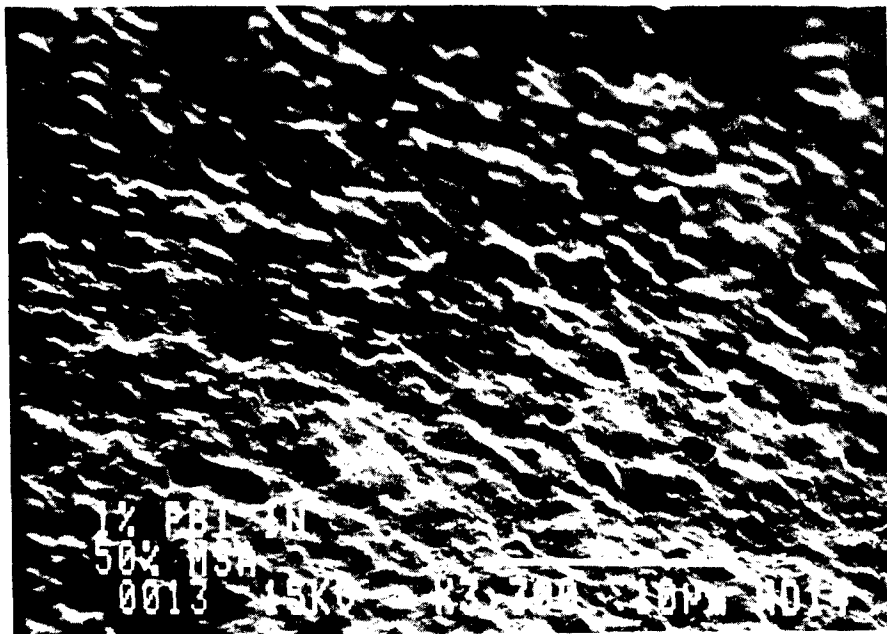


**Figure 11.** Scanning Electron Micrograph of a PBZT Film - Hand Sheared and Coagulated in a 50/50 MSA/Water Non-Solvent.

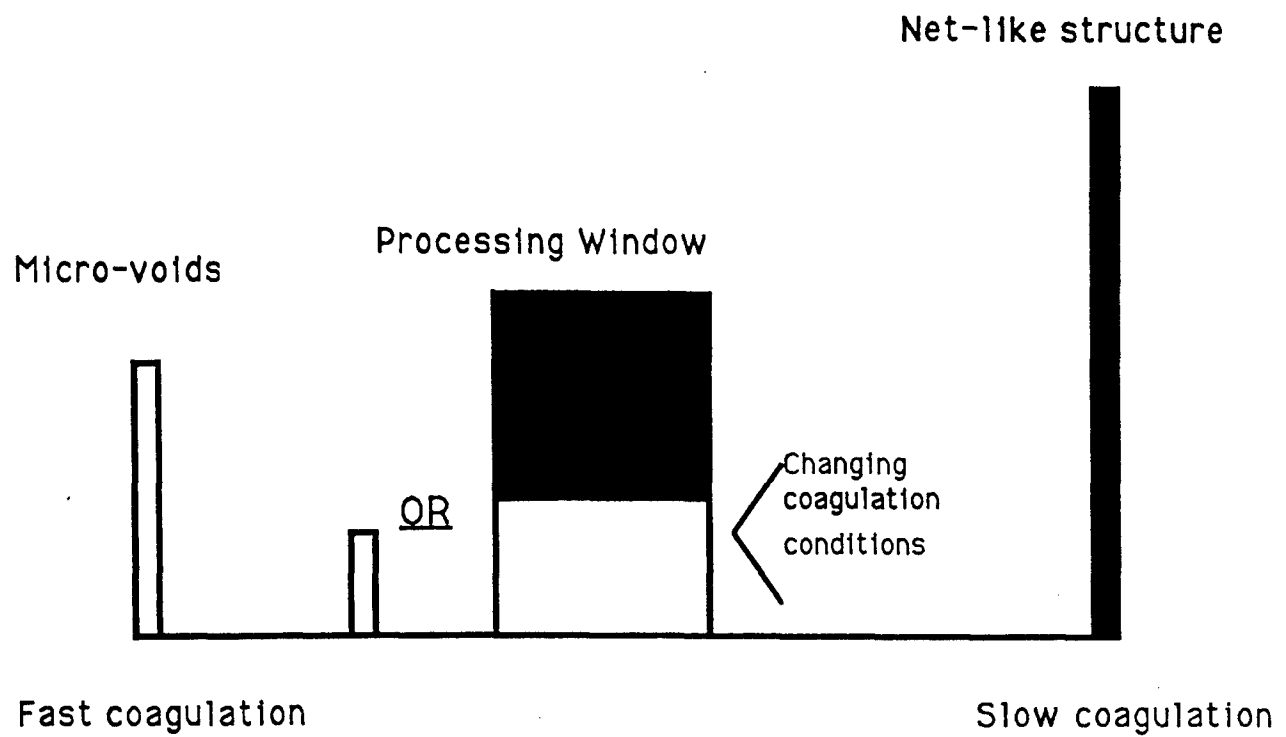


**Figure 12.** Processing Window Concept for Achieving Low Number-Density of Micro-Voids in the Slowly Coagulated Films.

**Table 3. List of Experiments for Coagulation of 1% PBZT/MSA Solution in 50/50 MSA/Water Non-Solvent.**

Non-Solvent	Coagulation Time	Micro-voids	Net-Like Structure
Water	5 mins. - 24 hrs.	Numerous	Nb
Air	0-10 min.	Nb	Yes
50% MSA/Water	24 hrs.	Few	Yes
50% MSA/Water	60 sec.	Few	Yes
50% MSA/Water	30 sec.	Few	Yes
50% MSA/Water	15 sec.	Few	Yes
50% MSA/Water	10 sec.	Few	Yes
50% MSA/Water - Air	10 sec./5 min.	Few	Yes
50% MSA/Water - Water	10sec./2 min.	Few	Yes
50% MSA/Water	5 sec.	Few	Yes
50%MSA/Water - Air	5 sec./5 min.	Few	Yes
50% MSA/Water-40%-30%-20%-10%	5 sec. each	Few	Yes
10% MSA/Water-20%-30%-40%-50%	5 sec. each	Numerous	Nb
50% MSA/Water - 10%	5 sec. each	Few	Yes
10% MSA/Water - 50%	5 sec. each	Numerous	Nb
All Acidic NS (described above) - Water	24 hrs.	Unchanged	Unchanged

micro-voids. To our knowledge this is the first report on the adverse affect of micro-void reduction achieved through changing the which were subsequently extruded coagulation conditions on the optical quality of the coagulated product.

### Classification of film samples on the basis of micro-void content

The casting thickness as well as the solvent content in the coagulation bath (initially zero) during the film extrusion are not strictly constant. Thus, it was expected that the various samples prepared from the same film extrusion would differ in the number density as well as in the size of micro-voids. Also, the micro-void number density was expected to be different in films of different compositions. This is because the thermodynamic phase equilibria between the polymer-solvent- non-solvent influences the micro-void formation (19). Thus, there was an interest in classifying the different film samples with respect to the micro-void number density. For this micro-void classification to be possible the micro-void density within the sample area (surface area of the largest film sample is 3 in<sup>2</sup>) should remain fairly constant. This was found to be true and it permitted the classification of samples into four categories with regard to the number of micro-voids (Table 4). Henceforth, this classification was used as a basis for the selection of samples which were sent out for NLO measurements.

### Macro-voids

The macro-voids are about 200 - 1000 microns in size and their number density is extremely small as compared to that of the micro-voids. They appear as bright spots when the sample is observed under cross-polars in an optical microscope (Fig. 13). It is interesting that this defect is absent in the films extruded from low viscosity solutions (1% PBZT, 5% 6F-PBO, 2% PBZT/Lubrizol-M, 4% PBZT-Thiophene and 2% PBZT/PBZT-Thiophene, in MSA). However, these features are also absent in the film extruded from a high viscosity dope of ABPBT/MSA and are present in extremely high concentration in the film extruded from moderately high viscosity 2% PBZT/6F-PBO in MSA. The origin of the macro-voids, thus, appears to be related to the viscosity of the extrusion solution and the nature of polymer. The possible causes for the macro-voids are: insufficient mixing, insufficient deaeration and lack of sufficient back pressure required to ensure the complete filling of the space in the extrusion flow channels, and also the nature of the polymer solution. The best way to avoid the macro-void formation, thus, is to keep the viscosity of the extrusion solution below about 2000-3000 Poise at  $1 \text{ s}^{-1}$ . It should be remarked that at such low viscosities, the shrinkage in the coagulated film would be considerable.

### Solid particles

The most common defect found in films, in general, is fisheyes or gels, also known as blobs. They consist of undissolved polymer particles which appear as small dark features (up to 30 microns in size) when examined under an optical microscope (Fig. 6). Currently,

**Table 4. Classification Scheme for Micro-Voids**

<b>Casting Thickness (microns)</b>	<b>Micro-void size (microns)</b>	<b>Number of Micro-voids (in 0.5 sq mm)</b>
25	40	10-20
12	<20	20-40
0.8	<10	<10



Figure 13. Optical Micrograph of a PBZT/6F-PBO Film Showing a Macro-Void.

a thin 30 micron screen is installed between the extrusion cylinder and the casting die. Not only is this setup inadequate in removing smaller particles but it also leads to an unsteady operation because of the cake buildup on the screen. An off-line filtering system (Appendix A-A3), which would be capable of removing 0.2 micron particles, has been constructed and is currently being installed.

### Lines in the transverse direction

High frequency lines can be visually observed during extrusion of all the films in the coagulation bath. They can also be observed under an optical microscope (Fig. 14). Among the ring mounted samples, only the 5% 6F-PBO samples show these lines in an optical microscope. However, when slide samples (film dried between two microscopic slides under tension) are viewed under cross-polarizers, the transverse lines can also be observed in the 3% PBZT/NYLON, 2% PBZT/NYLON and 2% 6F-PBO/PBZT samples. It is interesting to note that the films used for the slide samples and ring mounted samples were from the same extrusion. The fact that the transverse lines were not observed in the "good" ring mounted samples indicates that the drying configuration can obscure or eliminate this feature. Failure to observe these lines in most of the 1% PBZT samples might be due to the fact that the 1% PBZT film is especially thin. The spacing between the transverse lines in 5% 6F-PBO varies from 25 to 300 microns. Using the spacing and the extrusion film speed, the frequency of the cause(s) of these defects can be estimated. The frequency of these lines in 5% 6F-PBO samples

vary between 20 and 200 Hz, and in other films, it varies between 1 and 20 Hz. Also, it appears that there are two kinds of lines (Fig. 15) : the thicker one seems to be associated with small voids. When the samples were examined in the secondary electron imaging mode of the SEM, these lines could be seen only in the 5% 6F-PBO sample (Fig. 16).

It is possible that these lines are a manifestation of the gauge variation in the machine direction. Gauge variation in the machine direction can arise in three ways : 1. pulsation in the rate at which the dope is pumped (18, 25, 41); 2. uneven draw of the film (18); and, 3. insufficient resistance in the die resulting in a failure to develop the positive flow pattern (41).

An encoder - feedback speed control system was installed to regulate the piston speed. Also, a ten fold increase in the control of the casting roller speed was achieved. Both these improvements failed to remove the transverse lines. Currently, a new casting roller with significantly reduced wobbling is being installed. Also, a new die is being built. The optimization of the die design is based on the rheology of a number of polymer solutions which are expected to be extruded for Non-Linear Optics studies.

### Lines in the machine direction

The lines in the machine direction can be observed in all the films through the optical microscope (Fig. 17) and SEM (Fig. 18). For a film extruded at room temperature, gauge variation in the transverse direction arise primarily because of an uneven flow of the



**Figure 14.** Optical Micrograph of a 6F-PBO Film Showing the Lines  
in the Transverse Direction.

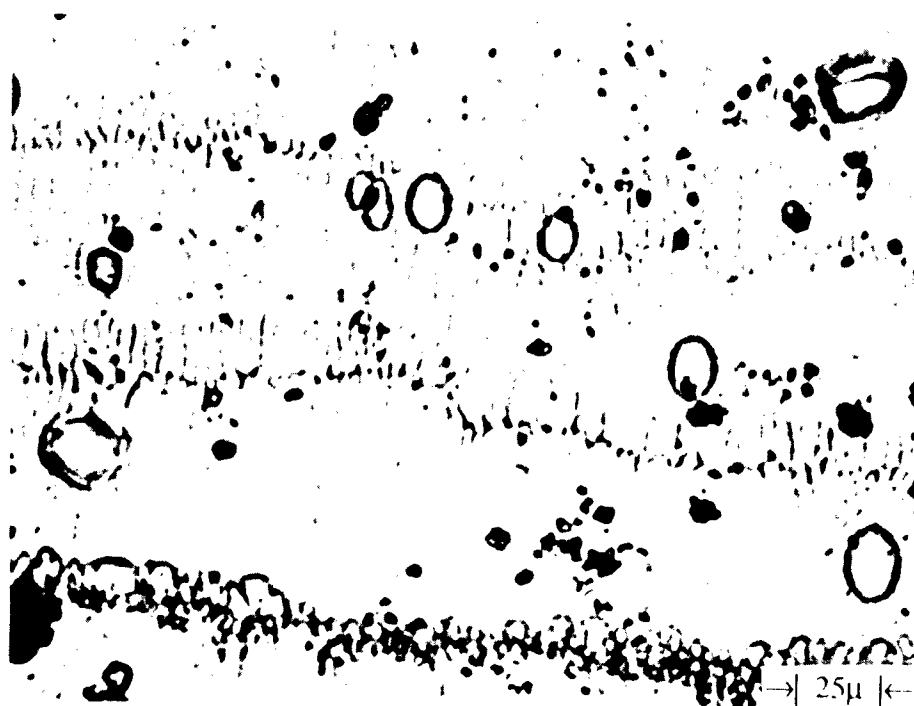


**Figure 15.** Optical Micrograph of a 6F-PBO Film Showing  
Two Different Kinds of Lines in the Transverse Direction.

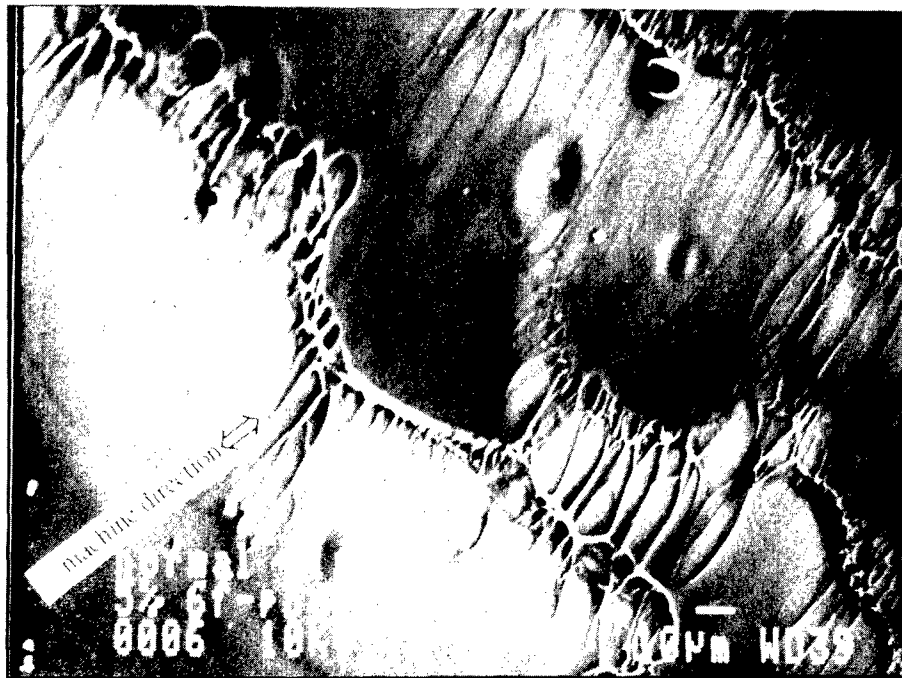


**Figure 16.** Scanning Electron Micrograph of a 6F-PBO Film Showing the Lines in the Transverse Direction.

polymer solution across the die which is related to an improper die design. Inappropriate design of the manifold, insufficient land region, bending of the die walls by pressure (non-uniform lip gap), nicks on the die lips, poor surface finish of the flow surfaces (in the die and also on the casting roller) and gauge variation in the machine direction can lead to these 'die lines' , as they are commonly known (18, 25, 43). Since the die is used in a 'doctor-blade' configuration (the die is placed vertically above the roller and the casting film thickness is determined by the gap between the roller and the die) and a bulge of polymer solution is maintained on the casting roller (behind the die - relative to the extrusion direction), it is likely that the nicks on the die lips and the poor surface finish of the casting roller are the cause of the lines in machine direction.

In an effort to eliminate this defect, a new coat-hanger die having a much better surface finish, is being built. Also, casting rollers with 'mirror finish' surfaces are being installed.

In summary, two classes of optical defects were observed. Identification and classification of these defects will help in modifying the current technique to eliminate the defects and in characterizing the optical quality of the film specimens in our pursuit to improve the processing of heterocyclic aromatic polymers for NLO applications.



**Figure 17.** Optical Micrograph of a PBZT/6F-PBO Film Showing the Lines in the Machine Direction.



**Figure 18.** Scanning Electron Micrograph of a PBZT/6F-PBO Film  
Showing the Lines in the Machine Direction.

## REFERENCES

1. T. Helminiak, C. L. Benner, F. E. Arnold, and G. E. Hussan, US Patent No. 4,207,407 (1980).
2. D. N. Rao, J. Swiatkiewicz, P. Chopra, S. K. Ghoshal, and P. N. Prasad, Applied Physics Letters, 48, 1187 (1986).
3. M. Zhao, M. Saamoc, P. N. Prasad, B. A. Reinhardt, M. R. Unroe, M. Prazak, R. Evers, M. Sinsky, and J. Kane, Chemistry of Materials, 2, 670 (1990).
4. J. F. Wolfe, B. H. Loo, R. A. Sanderson, and S. P. Bitler, Materials Research Soc. Symp. Proc., 109, 291 (1988).
5. M. Dotrong, R. C. Tomlinson, M. Sinsky, and R. C. Evers, Polymer Preprints, 1 (April 1990).
6. C. W. Spangler, T. J. Hall, L. S. Sapochak, and P. K. Liu, Polymer, 30, 1169 (1989).
7. S. Venkatraman, R. S. King, R. Furukawa, C. C. Lee, E. F. Casassa, and G. C. Berry, "Physical Chemical Studies of Polymers with Rod-Like Backbone Elements", AFWAL-TR-80-4099 (1980).
8. R. Lusignea, "Advanced Polymer Utilization", AFWAL-TR-84-4080 (1980).
9. T. E. Hwang, D. R. Wiff, C. Verschoore, G. E. Price, T. E. Helminiak, and W. W. Adams, Polymer Engineering and Science, 23, 784 (1983).

10. Private Communications : P. N. Prasad, (State University of New-York), L. Dalton, (University of Southern California), G. Stegman, (University of Arizona), Altman (Lockheed, LMSC).
11. T. Kaino, Jpn. J. Applied Physics, 24, 1661 (1985).
12. M. Dotrong, M. H. Dotrong, R. C. Evers, and G. J. Moore, ACS Preprints, 675 (Fall 1990).
13. W. F. Hwang, D. R. Wiff, T. E. Helminiak and W. W. Adams, Org. Coat. Plast. Chem. Preps., ACS Div. Org. Coat. Plast., 48, 929 (1983).
14. L. S. Tan and F. E. Arnold, in press.
15. Laboratory records.
16. P. J. Flory, Macromolecules, 11, 1138 (1978).
17. Y-C. C. Lee, W. Huh, and S. J. Bai, "Ternary Phase Diagrams of PBZT/ZYTEL 330/MSA and PBZT/LUBRIZOL/MSA Solutions", WRDC-TR-90-4017 (1990).
18. J. L. Hecht, in The Science and Technology of Polymer Films. Vol.1, Ed. O. J. Sweeting, Wiley-Interscience, New-York (1968).
19. A. Ziabicki, Fundamentals of Fiber Formation, Wiley-Interscience, New-York (1970).
20. R. B. Bird, W. E. Stewart, and E. N. Lightfoot, Transport Phenomena, Wiley-Interscience, NY (1960).
21. J. H. Perry, C. H. Chilton, and S. D. Kirkpatrick, Chemical Engineer's Handbook, McGraw-Hill Book Company, New York (1963).
22. P. V. Danckwerts, Gas-Liquid Reactions, McGraw -Hill International Book Co., NY.

23. W. L. McCabe and J. C. Smith, Unit Operations In Chemical Engineering, McGraw-Hill International Book Company, New Delhi (1976).
24. J. C. Slattery, Doctoral Thesis, Univ. of Wisconsin (1959).
25. Z. Tadmor and C. G. Gogos, Principles Of Polymer Processing, Wiley-Interscience, New-York (1979).
26. J. R. Minter, "Structural Investigation of Fibers and Films of Poly(P-Phenylene benzobisthiazole)," AFWAL-TR-82-4097, Vol. 1 (1982).
27. M. A. Druy, Technical Report II, AFW-5240-FM-8784-174 (1990).
28. D. R. Paul, Journal of Applied Polymer Science, 12, 383 (1986).
29. M. Takahashi and M. Watanabe, Sen- I Gakkaishi, 16, 545 (1960).
30. J. Cypryk, Polimery, 11, 214 (1966): 12, 119 (1967).
31. J. P. Knudsen, Textile Res. J., 33, 13 (1963).
32. V. L. Tsiperman et al., Khimicheskiye Vollkna, 2, 10 (1968).
33. V. Grobe, G. Mann and G. Duwe, Faserforschung u. Textiltech., 17, 142 (1966).
34. H. Takeda and Y. Nukushina, Kogyo Kagaku Zasshi, 67, 626 (1964).
35. G. Mann and V. Grobe, Faserforschung u. Textiltech, 17, 315 (1966).
36. O. I. Nachinkin, Khimicheskiye Vollkna, 4, 62 (1969).
37. K. E. Perepelkin and O. I. Nachinkin, Khimicheskiye Vollkna, 2, 19, (1964).
38. G. C. Berry, C. P. Wong, S. Venkatramen and S. G. Chu, AFML-TR-79-4115 (1979).

39. Y. Cohen, H. H. Frost, and E. L. Thomas, in Reversible Polymer Gels and Related Systems, Ed. P. S. Russo, ACS, Washington D.C., (1987).
40. J. F. Wolfe, in 'Molecular and Polymeric Optoelectronics Materials : Fundamentals and Applications,' SPIE, Vol. 682 (1986).
41. V. G. Anthony and C. L. Mantell, Polypropylene Fibers and Films, Plenum Press, NY (1965).
42. A. L. Griff, Plastics Extrusion Handbook, Reinhold Pub. Corp., NY (1962).
43. Y. Matsubara, Polymer Engineering and Science, 20, 716 (1980).

**APPENDIX A**

**Calculation of the pressure drop through the porous  
metal filters**

## Modeling of pressure drop through porous metal filters

**A.** Modeling as friction flow through a bed of solids:

In a porous metal plate, the individual metal particles are metallurgically bonded to their neighbors resulting in a coherent matrix with interconnected porosity (Fig. A-1). Thus, the porous plate can be considered as a bed of packed solids.

**B.** The pressure drop through a bed of solids for a newtonian fluid is given by Ergun equation (ref.23):

$$-\Delta P_f = \frac{K_1}{g_c} \left( (1 - \epsilon) \frac{S_p}{V_p} \right)^2 \mu u L \quad \dots\dots\dots \text{Eq. 3}$$

where :

$K_1 = 150/36$  (experimental value)

$\epsilon$  = porosity of bed

$S_p$  = surface area of one particle

$V_p$  = volume of one particle

$L$  = depth of the bed

$\mu$  = newtonian viscosity of the fluid

$u$  = linear filtrate viscosity

$-\Delta P_f$  = pressure drop over the bed

$g_c = 32.174 \text{ lb-ft/s}^2\text{-lb}_f$

### Assumptions in the Ergun equation

1. Actual channels may be effectively replaced by a set of identical parallel conditions, each of variable cross-section.
2. The mean hydraulic radius,  $r(h)$ , of the channels is adequate to account for the variations in channel cross-sectional size and shape.
3. Inertial forces are neglected.
4. The particles are packed at random with no preferred orientation of individual particles and all particles are of the same size and shape.
5. The fluid obey's Newtonian fluid constitutive equation.

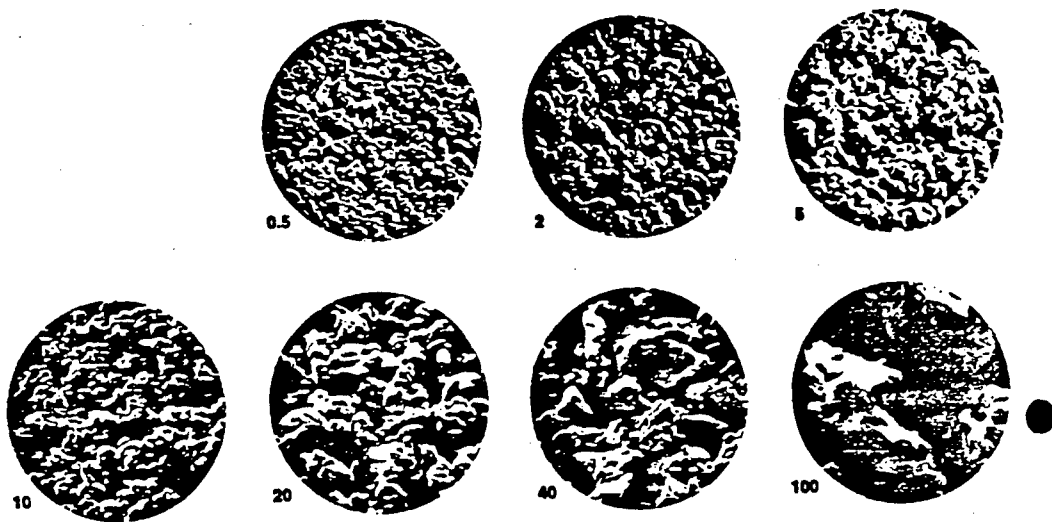


Figure A-1. 100X View of the Standard Mott Porous Metal Filters.

Limited pressure drop versus linear velocity plots are available (Fig. A-2). According to Eq. 1, for a porous plate of a given porosity and geometry, the pressure drop should be proportional to viscosity. For example, for the 0.5 micron plate, one can see from Fig. 20 that at a linear filtrate velocity of 0.8 GPM/Sq Ft,

$$\frac{\text{pressure drop for a 20 CP fluid}}{\text{pressure drop for a 5 CP fluid}} = 4$$

which is predicted by Eq. 1. However, similar viscosity dependence on the pressure drop is not seen at large viscosities or large linear filtrate velocity. The former is due to the fact that Eq. 3 is derived for a Newtonian fluid, and the latter is due to the fact that in Eq. 3 the inertia effects are neglected.

For our purpose, the inertial forces can be neglected since the linear filtrate velocities would be extremely small but the non-newtonian effects (shear dependence of the viscosity) will become highly significant due to the non-newtonian nature of the aromatic heterocyclic polymer solutions. The following expression has been derived for a power law fluid through a packed bed (Appendix A-2):

$$-\Delta P_f = \frac{K_1}{g_c} \left( (1-\epsilon) \frac{S_p}{V_p} \right)^{(1+n)} \eta_0 u^n L \frac{1}{\epsilon^{2n+1}} \dots \text{Eq. 4}$$

where:

$n$  : is the power law index, and

$\eta_0$  : is the viscosity at a shear rate of 1/s.

The validity of the equation can be seen from Fig. 20. The slope of log (pressure drop) vs. log ( $u$ ), at high viscosities, is significantly less than unity.

To find the value for the expression:

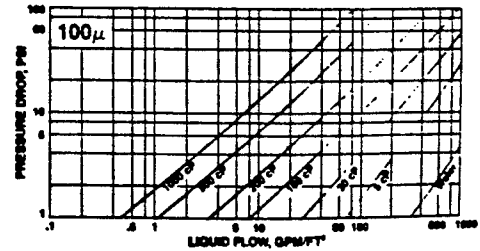
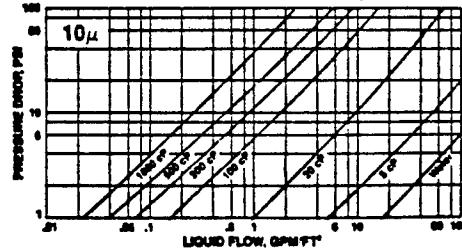
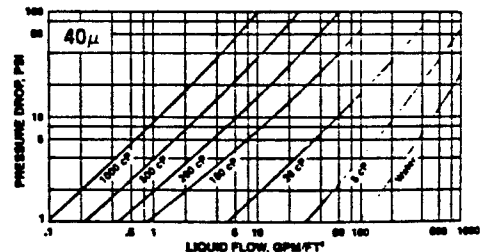
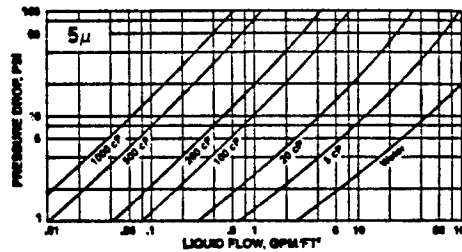
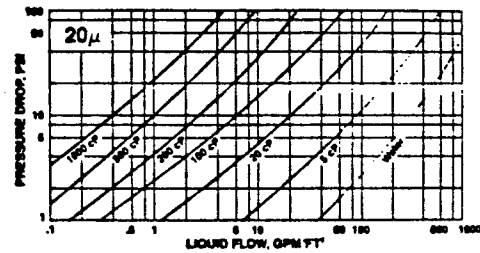
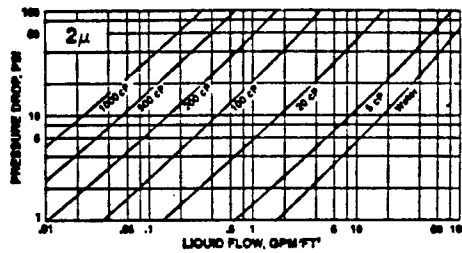
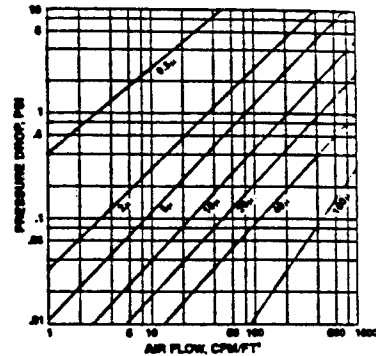
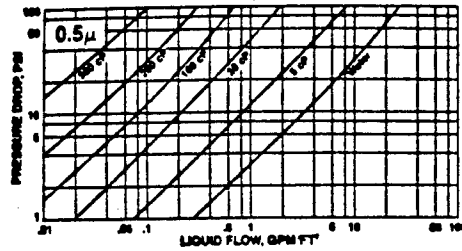
$$\left( (1-\epsilon) \frac{S_p}{V_p} \right)^{(1+n)} \frac{1}{\epsilon^{(2n+1)}}$$

assume:

$$\left( (1-\epsilon) \frac{S_p}{V_p} \right)^{(1+n)} \frac{1}{\epsilon^{(2n+1)}} = \frac{\left( (1-\epsilon) \frac{S_p}{V_p} \right)^2}{\epsilon^3}$$

The RHS of the above expression can be found from Eq. 3 and Figure A-2, from the limited region where Eq. 3 applies. Since the

These flow curves are presented as a design aid, to help in the development of filter applications using Mott porous sheet media. Flow data for water and higher viscosity liquids are given in the graphs below, organized according to the seven standard micron grades; the air flow graph at right has data for all micron grades, determined under ambient conditions.



**Notes to Flow Graphs**

- Standard sheet thickness varies with micron grade as follows: 0.5 micron .047" thick; 2, 5, 10 & 20 micron .062" thick; 40 micron .078" thick; 100 micron .083" thick.
- Flow curves are presented in a log-log format; be sure to note correct numerical values for each log cycle.
- Flow characteristics given are for porous media only. To determine total pressure drop of a system, combine losses through media, fittings, housing, piping and valves as appropriate.
- These flow characteristics were derived using 316L SS porous media. They are structure-related, not material-related, hence they apply to all available alloys.
- Liquid flow data were generated using water for viscosity of one centipoise and silicone oil for all higher viscosities.
- These flow characteristics are typical and should be used for general reference only.

Figure A-2. Flow Characteristics of Mott Porous Metal Filters.

constant  $K_1$  in Eq. 3 and Eq. 4 is an experimental parameter (found from experiments on real fluids), the error introduced due to the above assumption should be small. The value of this expression was calculated for 0.5  $\mu$ , 2  $\mu$ , 5  $\mu$ , 10  $\mu$ , 40  $\mu$ , and 100  $\mu$  porous plates. The expressions for the pressure drop as a function of viscosity,  $n$ ,  $L$  and  $u$  are tabulated in Table A-1.

One can see that there is a drastic effect of filtration time (proportional to linear filtrate velocity) and power law index,  $n$ , on the pressure drop. The converse is also true, namely, if the capability of the filtration system to generate and tolerate pressure is increased two folds, then for the same fluid, the filtration time is decreased by a factor of  $2^{1/n}$ . Consideration of the slow speeds achievable through the existing screw-jack in the laboratory, viscosity range of the low concentration methane sulphonic acid solutions and the pressure generating capability of the existing screw jack revealed that porous metal filter would be a suitable choice for the filtration of the heterocyclic aromatic NLO polymers. In addition, if the temperature capability is added to the filtration system, then it could also be used for the Polyphosphoric acid solutions.

**Table A-1 Pressure Drop for Mott Filters.**

Filtration Grade ( $\mu$ )	$\frac{K_1}{\epsilon_c} ((1-\epsilon) \frac{S_p}{V_p})^2 \frac{L}{\epsilon^3} \left( \frac{s^2 \cdot \text{lb}_f}{\text{lb} \cdot \text{ft}^2} \right)$	$(-\Delta P_f) \frac{\text{lb}_f}{\text{in.}^2}$
	$\times 10^4$	$\times \mu_0 \left( \frac{u}{720} \right)^n \cdot L$ ●
0.5	10110	4255
2.0	1853	887
5.0	1122	537
10	168	81
20	92	44
40	27	10
100	6	1

● u : inches/minute  
 L : Inches - height of the porous plate

**APPENDIX A1**  
**Expression for the pressure drop of a Non-Newtonian fluid through a porous plate**

## Modeling of a power-law fluid through a porous media

As stated in Appendix A, all the assumptions involved in the derivation of the Ergun equation (Eq. 3, Appendix A) apply in our case except the assumption of fluid following Newtonian viscosity behavior. The fluids which would be filtered almost always follow Non-Newtonian behavior. Thus, the need to develop an expression for the pressure drop through a porous media for a Non-Newtonian fluid.

The velocity distribution in a tube of radius, R, is given by (ref.23)

$$V(r) = \left(\frac{R}{s+1}\right) \left(\frac{-R}{2\eta_0} \frac{dP^s}{dz}\right) \left(1 - \left(\frac{r}{R}\right)^{s+1}\right)$$

where all the symbol are same as defined in Eq. A -

$$\text{Appendix A1, } s = \frac{1}{n}$$

From the z component (in the direction of flow) of the equation of motion and from the boundary condition : at r = 0, shear stress component  $\tau_{rz} = 0$ , it follows that,

$$\tau_w \text{ (shear stress at } r = R) = -(R/2) \frac{dP}{dz}$$

Therefore,

$$V(r) = \left(\frac{R}{s+1}\right) \left(\frac{\tau_w^s}{\eta_0}\right) \left(1 - \left(\frac{r}{R}\right)^{s+1}\right)$$

The average velocity,  $V_a$ , is given by:

$$V_a = \frac{1}{\pi R^2} \int V(r) \times 2\pi r \, dr$$

or 
$$V_a = \left(\frac{\tau_w}{\eta_0}\right)^s \left(\frac{R}{s+3}\right)$$

$$\tau_w = V_a^{\left(\frac{1}{s}\right)} \mu_0 \frac{1}{R^{\left(\frac{1}{s}\right)}} (s+3)^{\left(\frac{1}{s}\right)}$$

Rewriting the above equation in terms of the hydraulic radius,  $r_h$ ,

$$\tau_w = K_1 \mu_0 V_a \left(\frac{1}{s}\right) \frac{1}{r_h \left(\frac{1}{s}\right)}$$

(Note that we will use the same value of  $K_1$  as in the Ergun equation, i.e.  $K_1 = 150/36$ , in this equation. When the expression for  $\tau_w$  is written in terms of hydraulic radius, a factor of 8 is replaced by  $K_1$ . But since  $K_1$  is an experimental value, we will assume that the same value can be used to replace  $2^{1/s} (s+3)^{1/s}$  when the expression for  $\tau_w$  is written for the hydraulic radius.)

The velocity,  $V_a$ , is the average velocity through the channels in the filter media. If  $u$  is the filtrate velocity, then

$$V_a = u/\epsilon$$

where  $\epsilon$  = porosity.

The total area,  $A$ , is given as  $A = NS$ ,

where  $N$  = total number of particles in the bed, and

$S$  = area of one particle.

If  $L$  is the total bed depth and  $S(o)$  the cross-section of the empty plate, the total volume of the solids is

$$N = S(o) L (1 - \epsilon) / V$$

Eliminating  $N$  from above two equations gives,

$$A = S(o) L (1 - \epsilon) S/V$$

The hydraulic radius is defined as the ratio of the conduit to the perimeter of the conduit. If the numerator and the denominator

of this ratio are both multiplied by  $L$ , the hydraulic radius becomes the ratio of the volume of the voids in the plate to the total area of the solids. The volume of the voids is  $S(o)L \epsilon$ . Therefore, using the above equation yields:

$$\text{Hydraulic radius, } r_h = S(o) \frac{L\epsilon}{A} = \frac{S(o)L\epsilon}{S(o)L(1-\epsilon) \frac{S}{P}} = \frac{\epsilon V}{(1-\epsilon)S}$$

Substitution of  $r_h$ ,  $A$  and  $V_a$  in the following force balance:

$$\tau_w = \frac{F_d}{A} = \frac{K_1 \mu_0 V_a \left(\frac{1}{s}\right)}{r_h \left(\frac{1}{s}\right)}$$

where  $F_d$  is the viscous drag force on the fluid.

$$\text{gives, } F_d = K_1 \mu_0 \left(\frac{u}{\epsilon}\right) \left(\frac{1}{s}\right) \left(\frac{(1-\epsilon)S}{\epsilon V}\right) \left(\frac{1}{s}\right) \frac{S(o)L(1-\epsilon)S}{V}$$

The pressure drop over the filter may be used in place of the total force.

$$F_d = -\Delta P_f \epsilon S(o) \quad (\text{neglecting the inertial forces}),$$

also, replacing  $s = 1/n$  gives

$$-\Delta P_f = \frac{K_1}{g_c} \left( (1-\epsilon) \frac{S_p}{V_p} \right) (1+n) \eta_0 u^n L \frac{1}{\epsilon^{2n+1}} \quad \text{.....Eq. 5}$$

This equation reduces to the Ergun equation (Eq. 3 in Appendix A) for  $n = 1$ , as expected. When working in FPS units, the right side of the equation should be divided by  $g_c$ .

**APPENDIX A2**  
**Design of the filtration system**

SCHEMATIC OF THE FILTRATION OPERATION

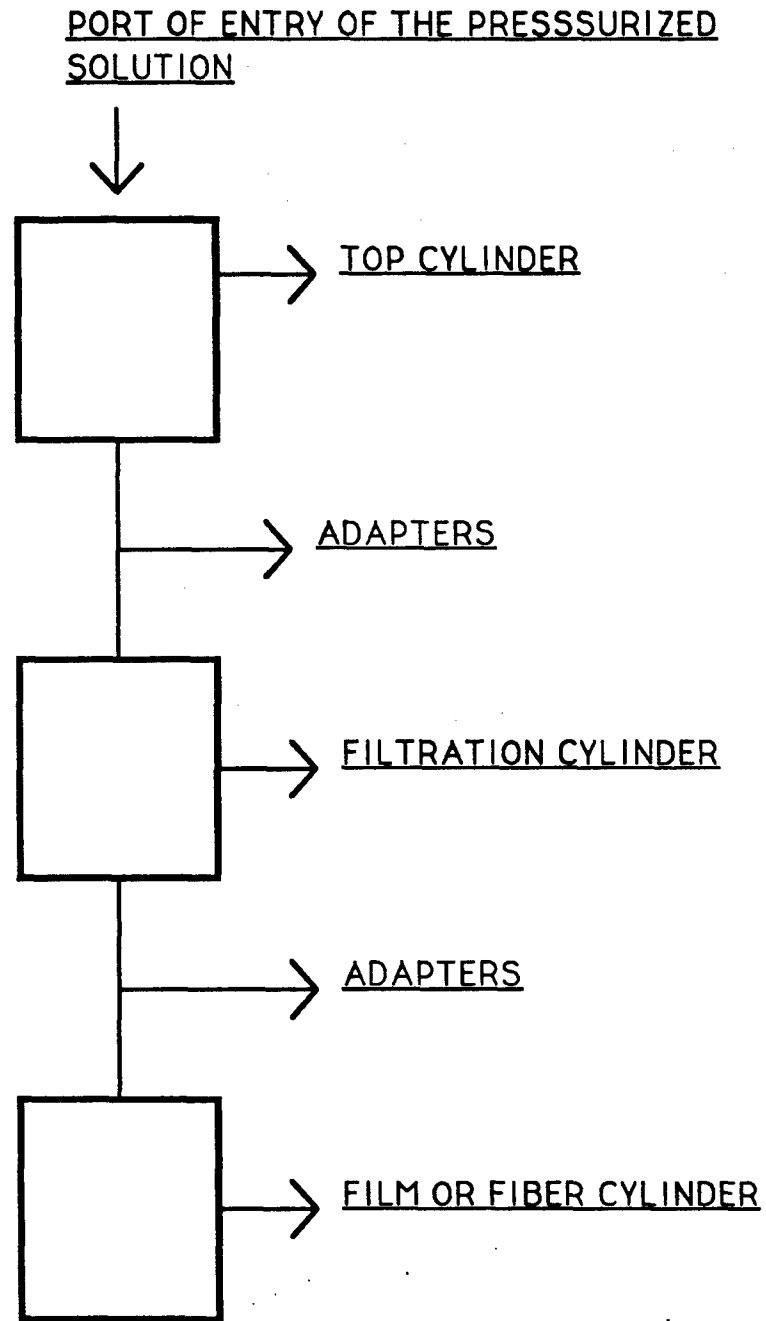
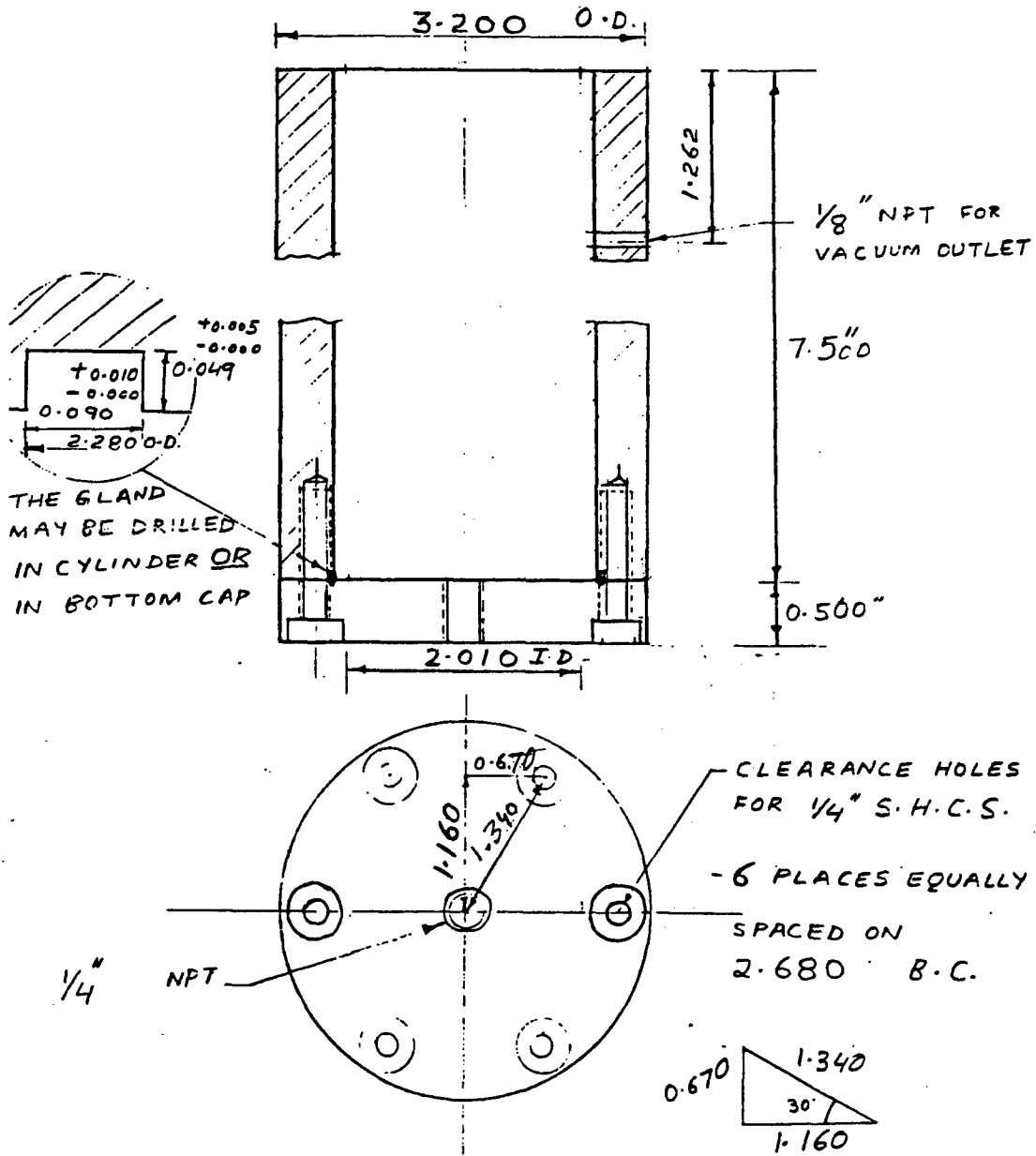


## TABLE OF CONTENTS

	<b>Page</b>
1. Top cylinder	71
2. Piston for the top cylinder	72
3. Supporting drawings for the piston for the top cylinder	73
4. Cap for the existing fiber extrusion cylinder	74
5. Cap for the existing film extrusion cylinder	75
6. 1" filtration cylinder	76
7. Top part of the 1" filtration cylinder	77
8. O-ring plate for the 1" filtration cylinder	78
9. Distributor and O-ring plate for the 1" filtration cylinder	79
10. 1/8 " spacer plates for the 1" filtration cylinder	80
11. 1/16 " spacer plate for the 1" filtration cylinder	81
12. 2.7" filtration cylinder	82
13. Top part of the 2.7 " filtration cylinder	83
14. O-ring plate for the 2.7 " filtration cylinder	84
15. Distributor and O-ring plate for the 2.7" filtration cylinder	85
16. 1/8 " spacer plates for the 2.7" filtration cylinder	86
17. 1/16" spacer plate for the 2.7 " filtration cylinder	87

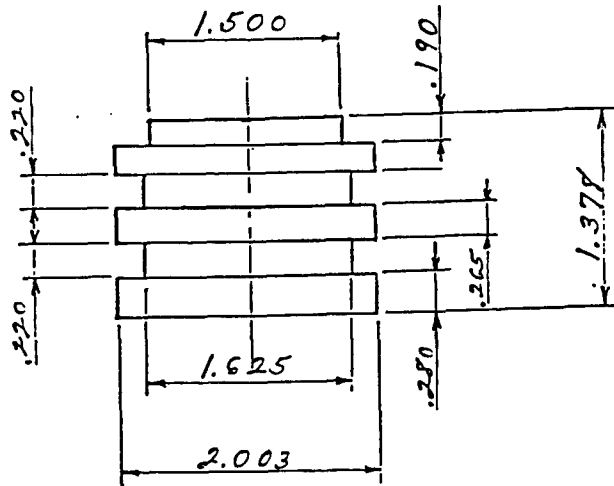
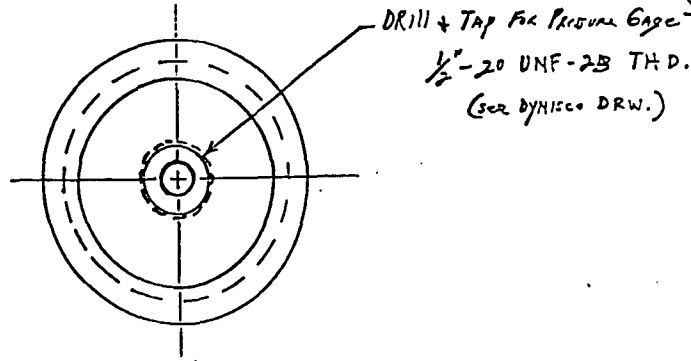
**Material of construction:** Carpenter 20 Cb 3 Stainless Steel

# Top cylinder



# Piston for the top cylinder

DYNISCO  
TPT 432 A



## Supporting drawings for the piston for the top cylinder

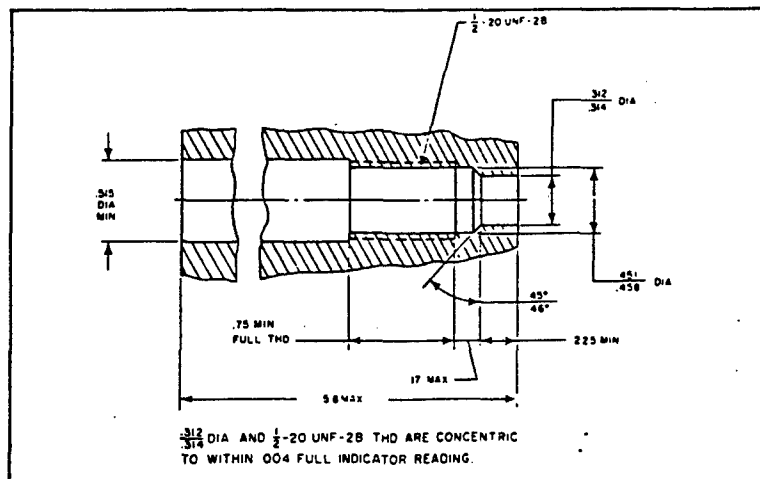
### SUGGESTED PROCEDURE

- Step 1 Drill a hole through with the 9/32" drill.
- Step 2 Ream the hole with the 5/16" reamer.
- Step 3 Consult the mounting hole drawing and calculate the depth required for the .451/.458" hole to leave .225" minimum length of the 5/16" (.312") diameter hole.
- Using the special 29/64" piloted drill, drill to the depth calculated above, perhaps leaving a little excess to be removed in Step 7.
- Step 4 Drill with the 17/32" drill, if necessary, so as to leave approximately 1" of the 29/64" diameter hole length.
- Step 5 Tap with the 1/2-20 Plug tap (tap with tapered lean) as deep as possible without striking the chamfered seating surface that was produced by the piloted drill.
- Step 6 Tap to the final depth with the 1/2-20 UNF bottoming tap.
- Step 7 Examine the seating surface of the mounting hole. If it has been marked by the tapping operation, touch it up with the piloted drill.

It is generally good practice to check the mounting hole before installing the transducer. One procedure is to coat a gauge plug (P/N 200908) with Dykem machine blueing on surfaces below the thread. Insert the gauge plug into the mounting hole and rotate until surface binding is encountered. Remove and inspect. Blueing should only be scraped off of the 45° sealing chamfer. If blueing has been removed from other surfaces, the mounting hole has not been machined properly.

**NOTE:** This kit contains premium grade cutting tools including cobalt HSS 9/32" and piloted drills. Care, however, should be taken in the use of proper speeds and feeds, lubricants, and a method to assure continual alignment of each progressing tool. Consult the factory if additional or more specific information is required.

### RECOMMENDED MOUNTING HOLE



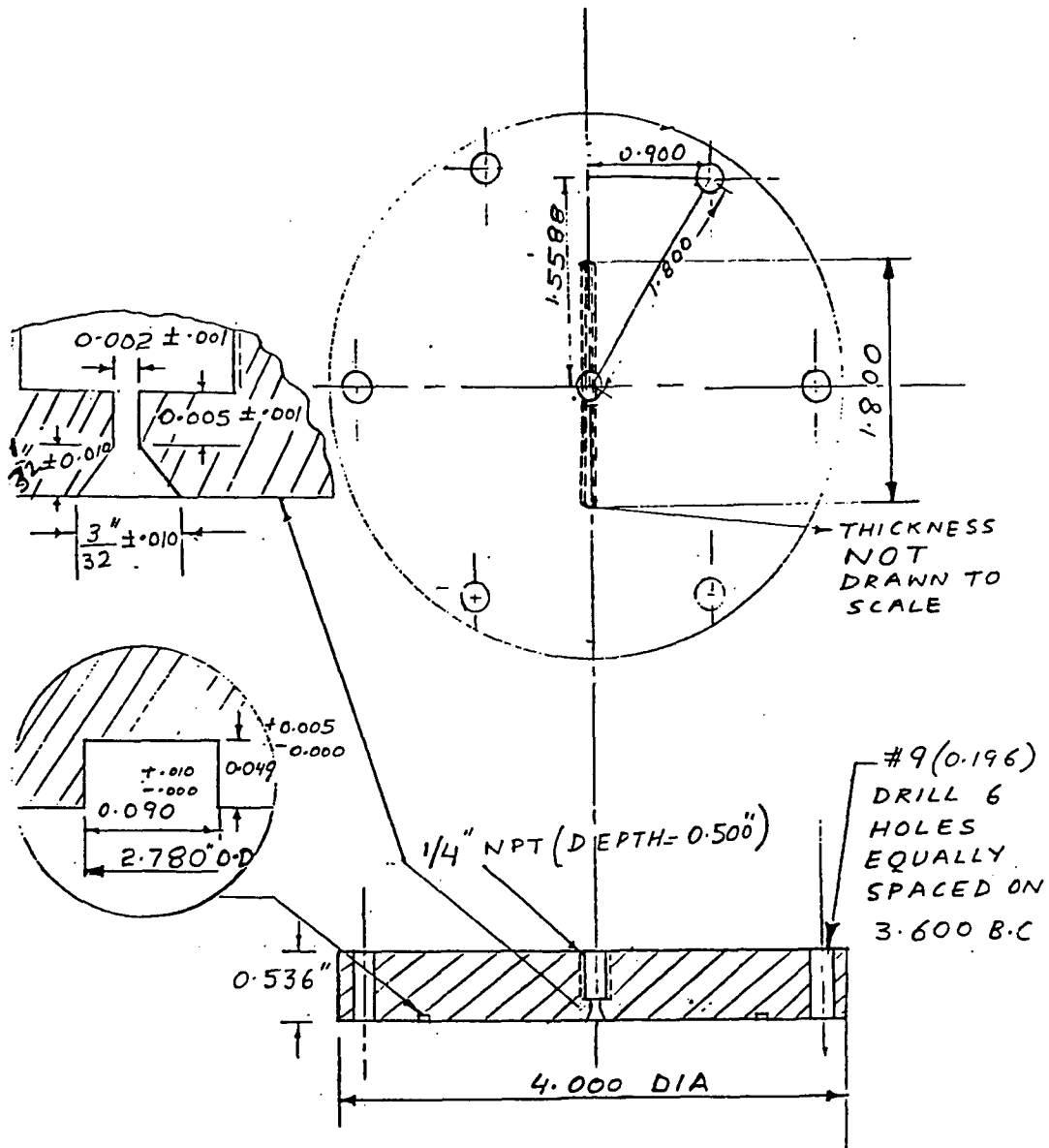
# Dynisco

20 Southwest Park, Westwood, Massachusetts 02090 Telephone: 617-326-8210 Telex: 092-4347

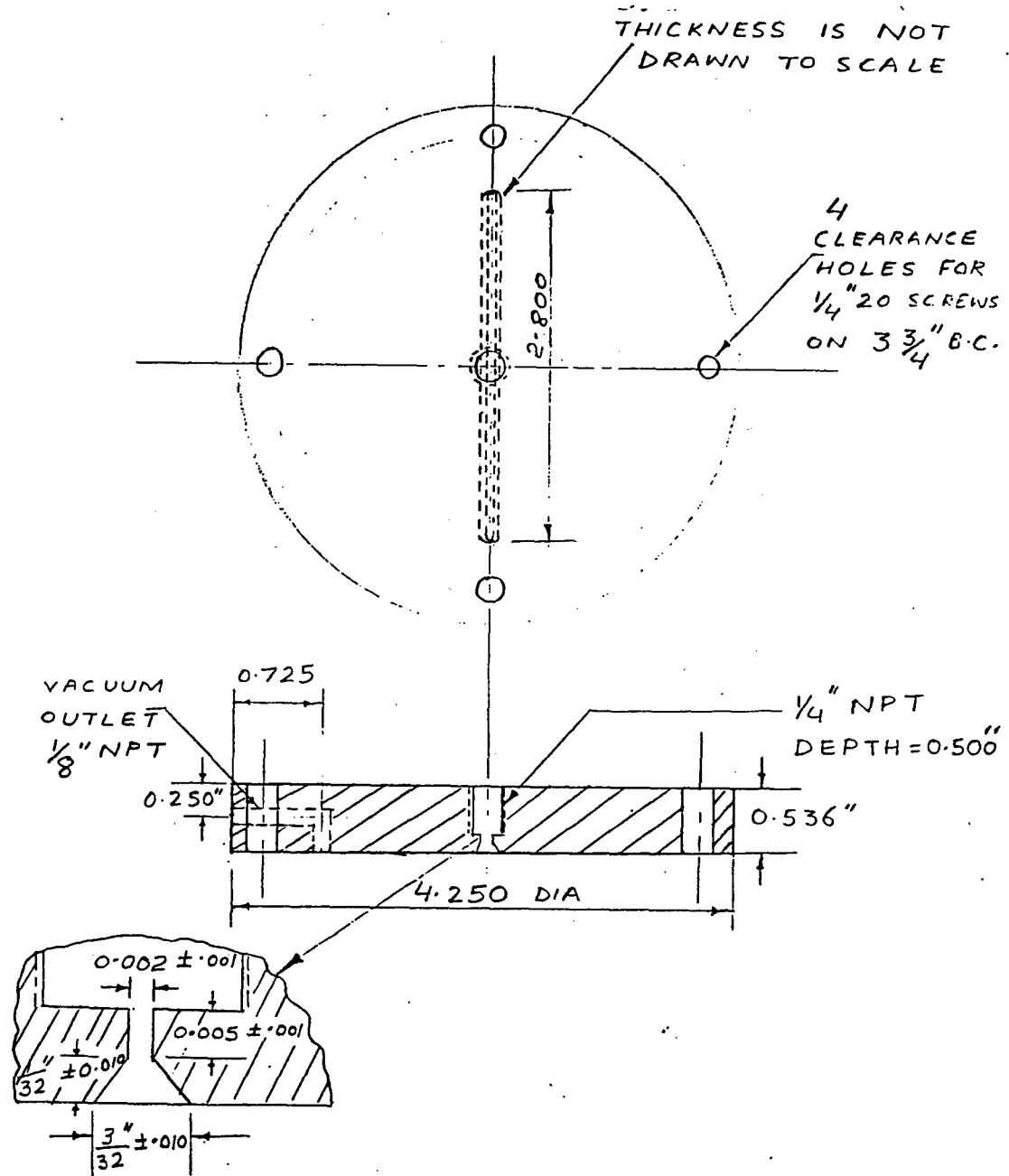
PRINTED IN U.S.A.

A BOFORS COMPANY

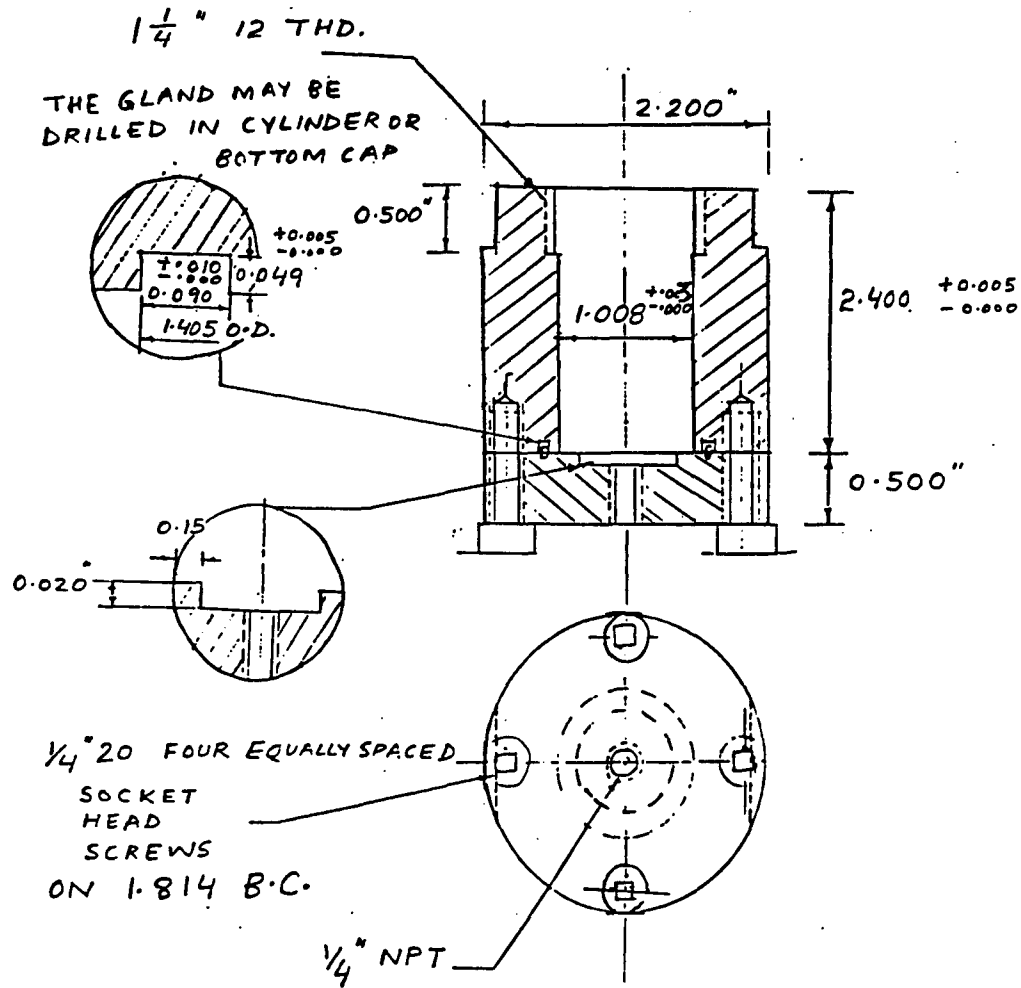
Cap for the existing fiber extrusion cylinder



# Cap for the existing film extrusion cylinder

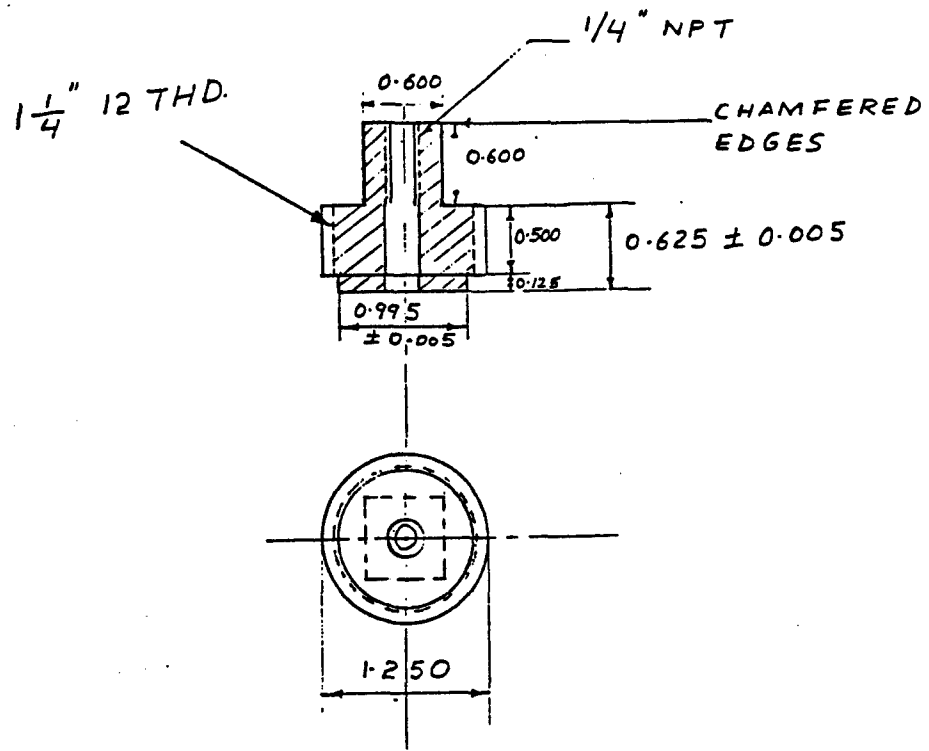


# 1" filtration cylinder

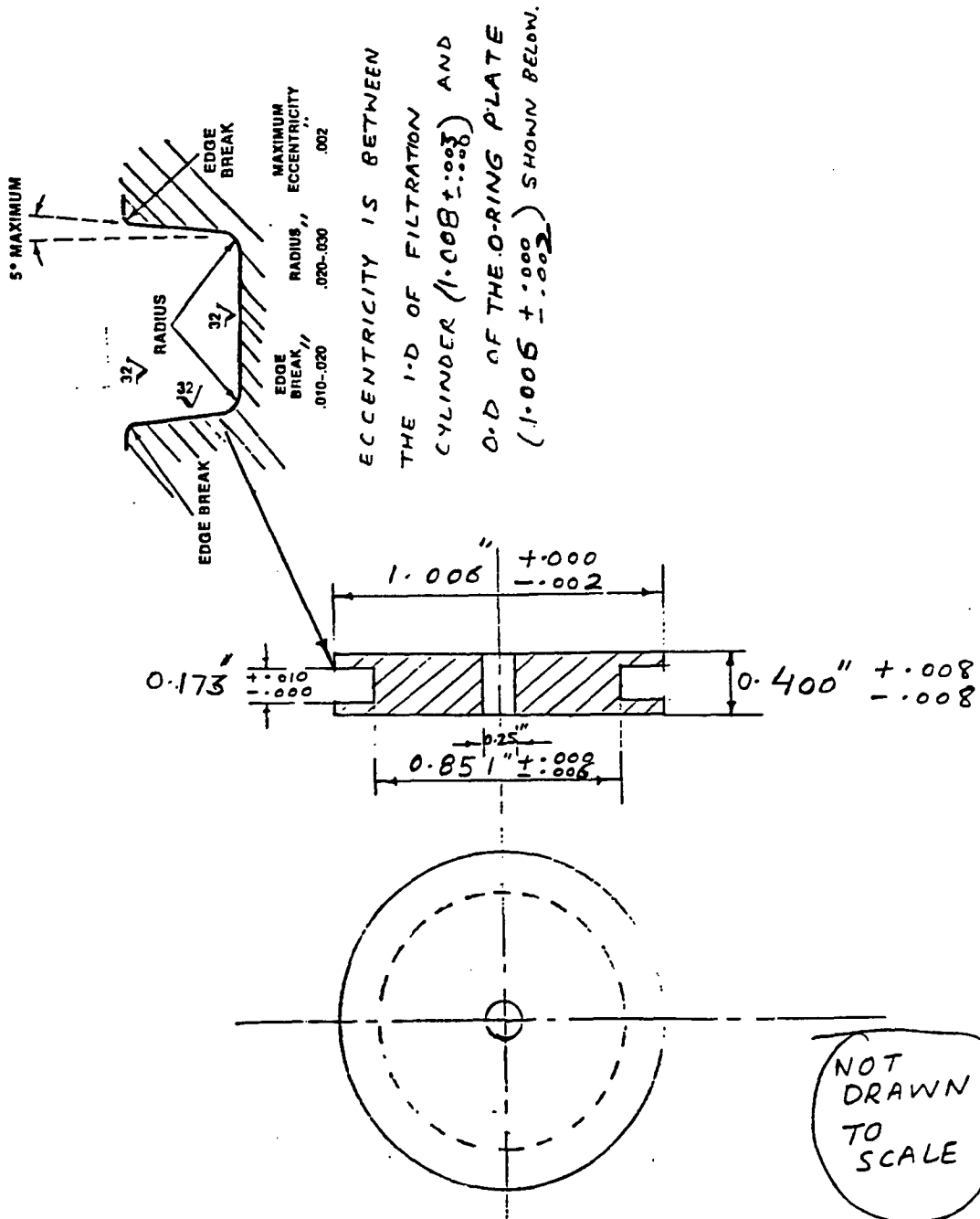


NOT DRAWN TO SCALE (HEIGHT OF THE CYLINDER)

Top part of the 1" filtration cylinder

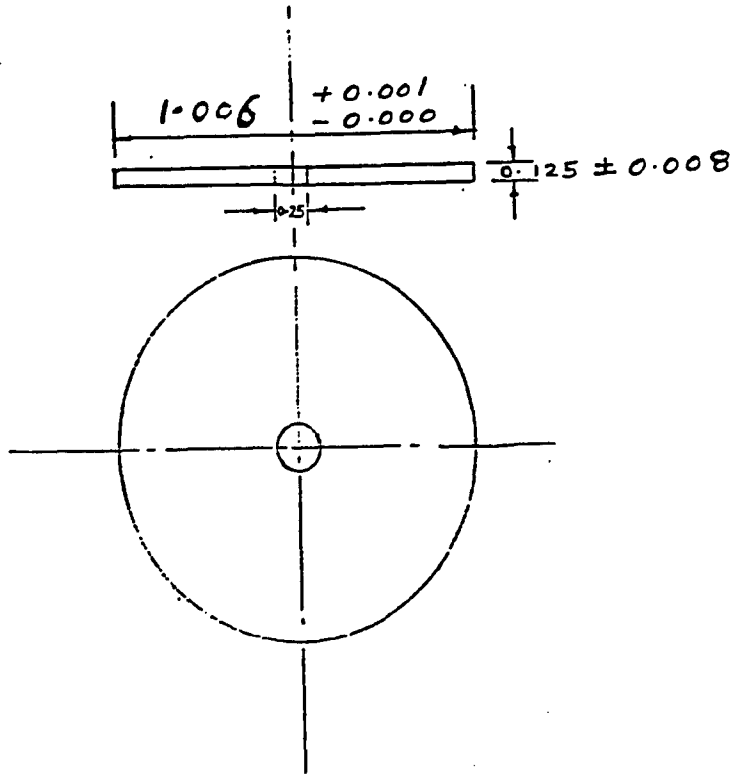


# O-ring plate for the 1" cylinder



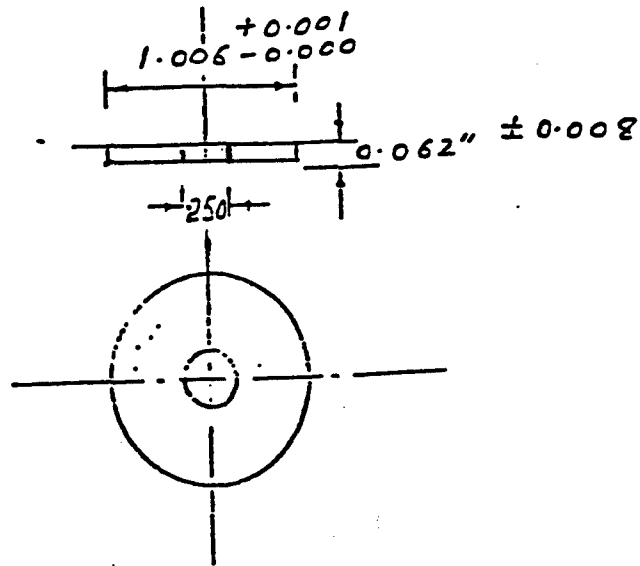


1/8" spacer plates for the 1" filtration cylinder

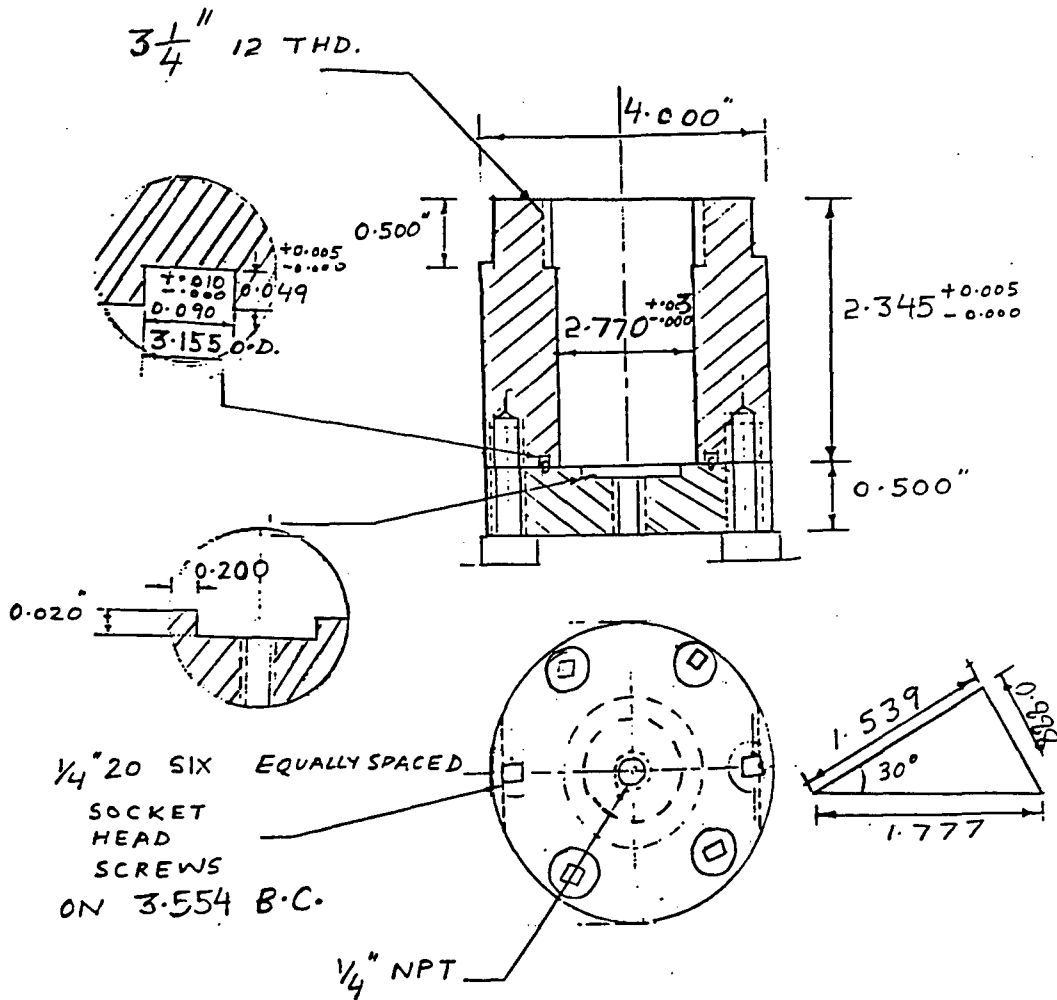


NOT DRAWN TO SCALE

1/16" spacer platte for the 1" filtration cylinder

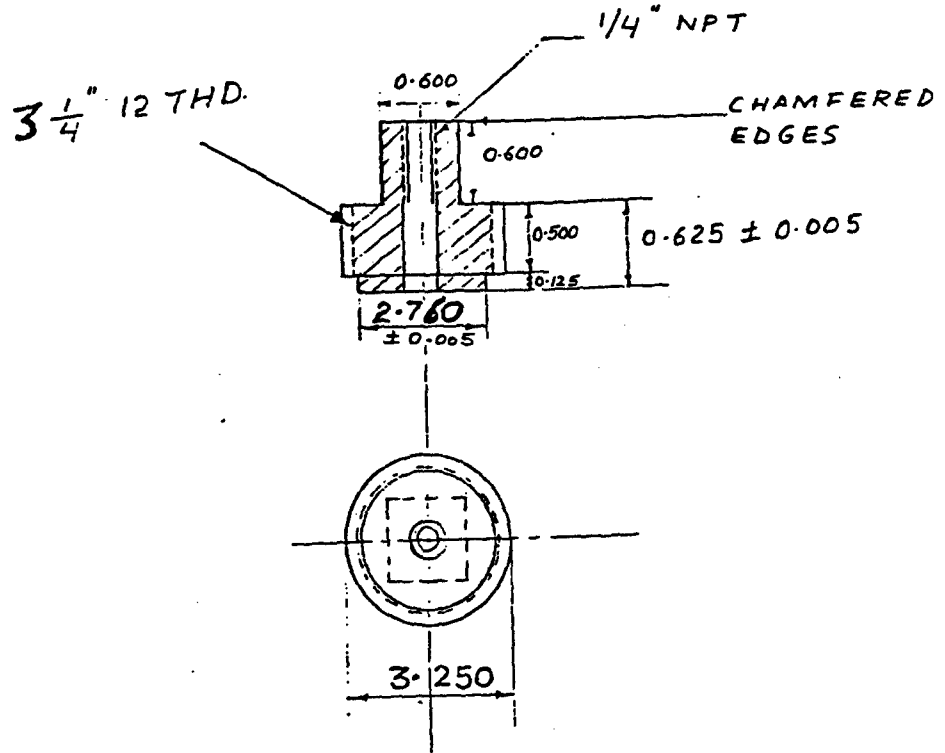


# 2.7" filtration cylinder



NOT DRAWN TO SCALE

Top part of the 2.7" filtration cylinder

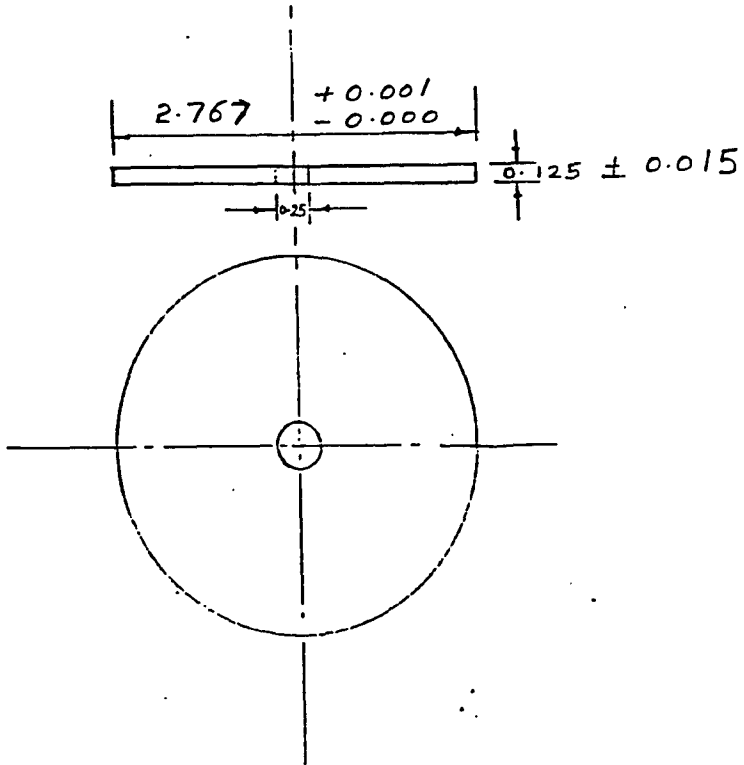


NOT DRAWN TO SCALE

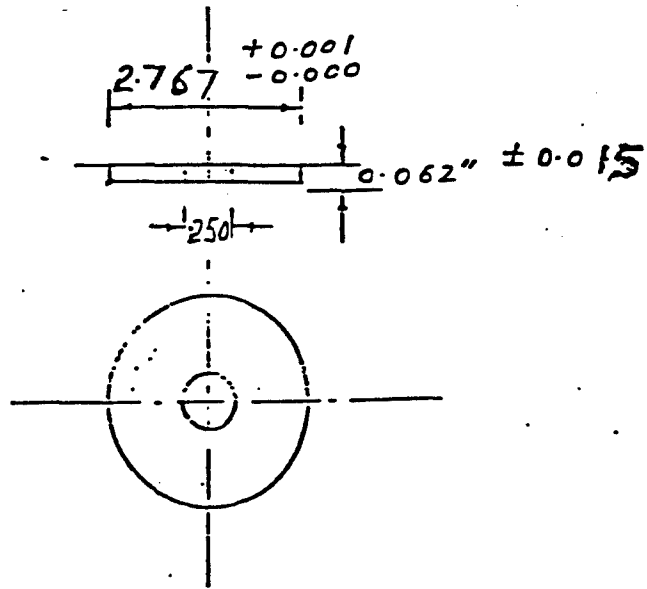




1/8" spacer plates for the 2.7" filtration cylinder



1/16" spacer plate for the 2.7" filtration cylinder

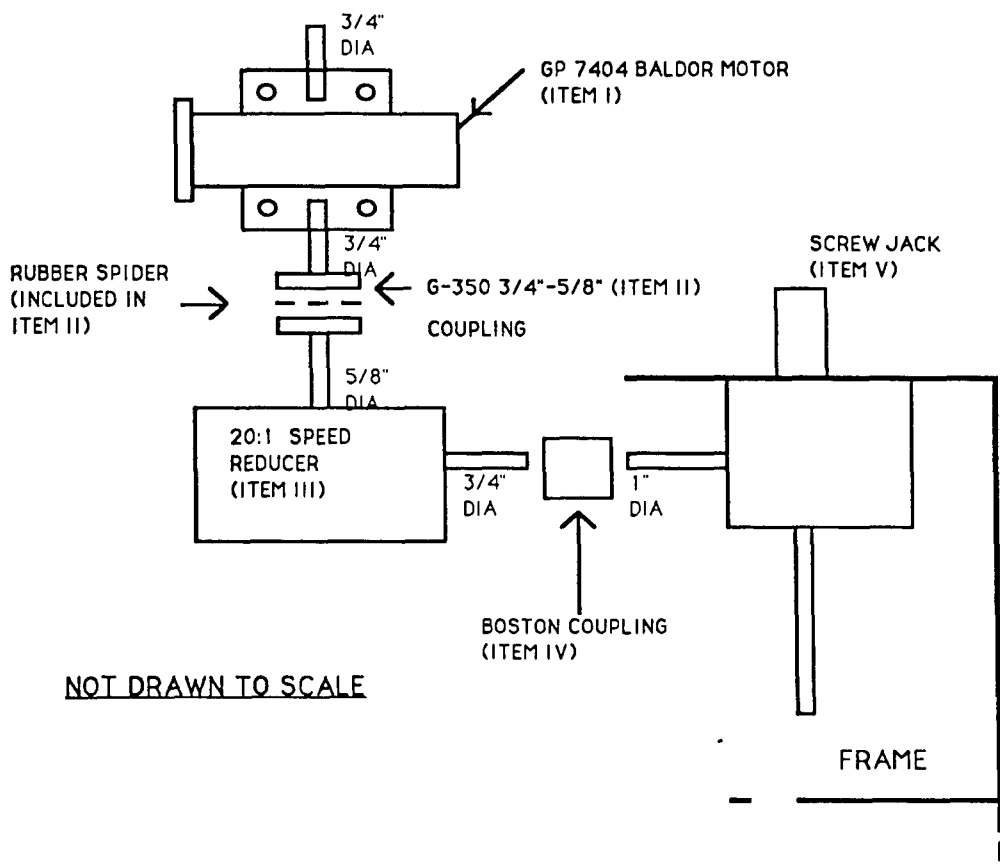


**APPENDIX A3**  
**Design of the frame for the filtration assembly**

## Table of contents

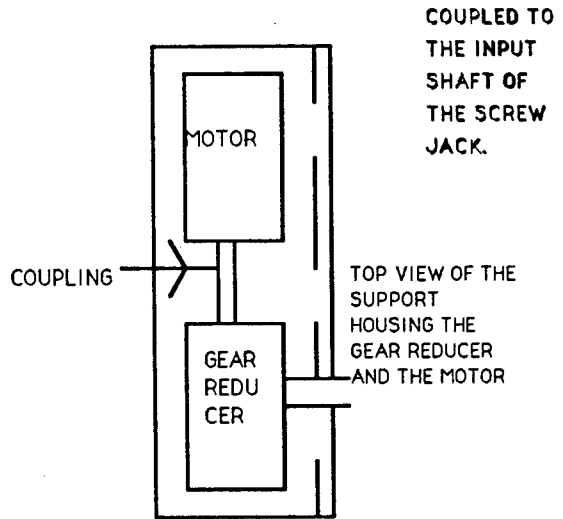
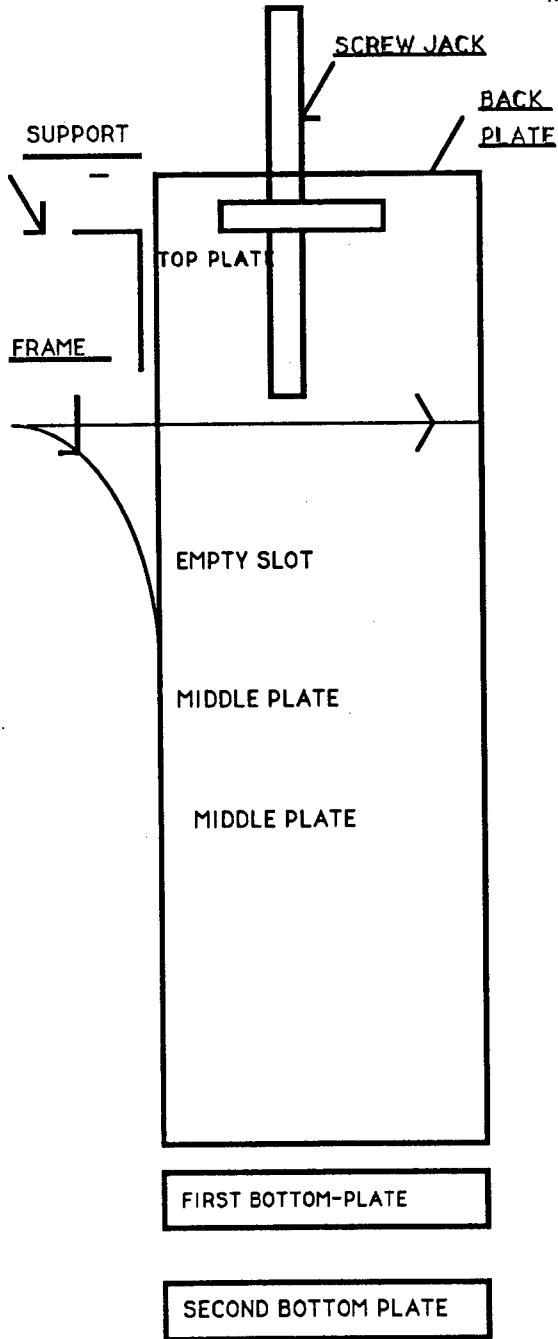
	<b>Page</b>
1. Overall schematic of the assembly	90
2. Schematic of the assembly of the frame unit	91
3. Frame and the back plate	92
4. Back-plate	93
5. Hole pattern in the frame and the back plate	94
6. Bottom view of the frame and the back plate	95
7. Top-plate	96
8. Middle-plate	97
9. First bottom-plate	98
10. Second bottom-plate	99
11. Support	100

Overall schematic of the assembly



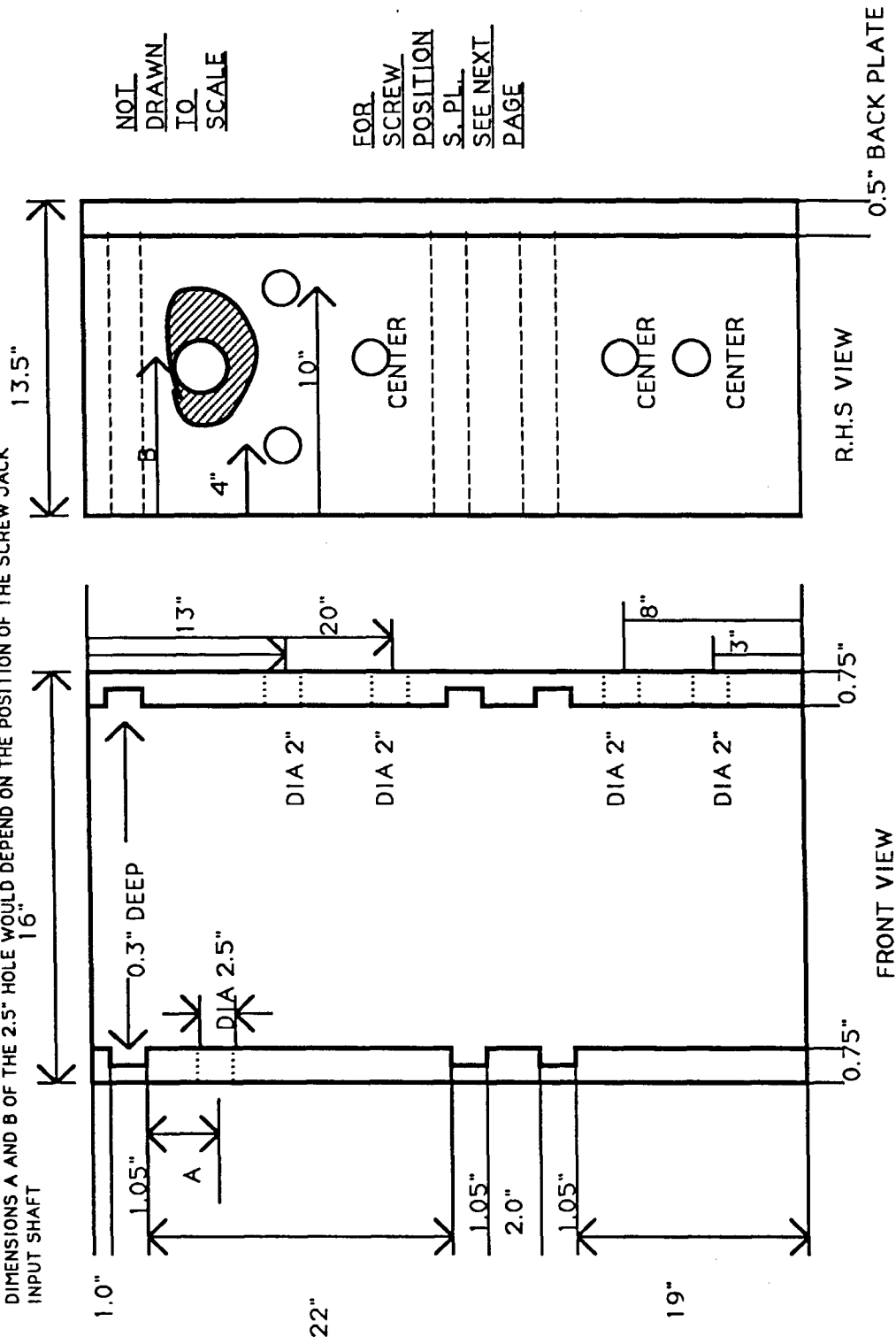
Schematic of the assembly of the frame unit

THE FRAME AND THE BACK PLATE WOULD REST ON THE FIRST BOTTOM PLATE, WHICH IN-TURN WOULD REST ON THE TEFLON PLATE



NOT  
DRAWN  
TO  
SCALE

DIMENSIONS A AND B OF THE 2.5" HOLE WOULD DEPEND ON THE POSITION OF THE SCREW JACK INPUT SHAFT



NOT  
DRAWN  
TO  
SCALE

FOR  
SCREW  
POSITION  
S. PL.  
SEE NEXT  
PAGE

Frame and the back plate

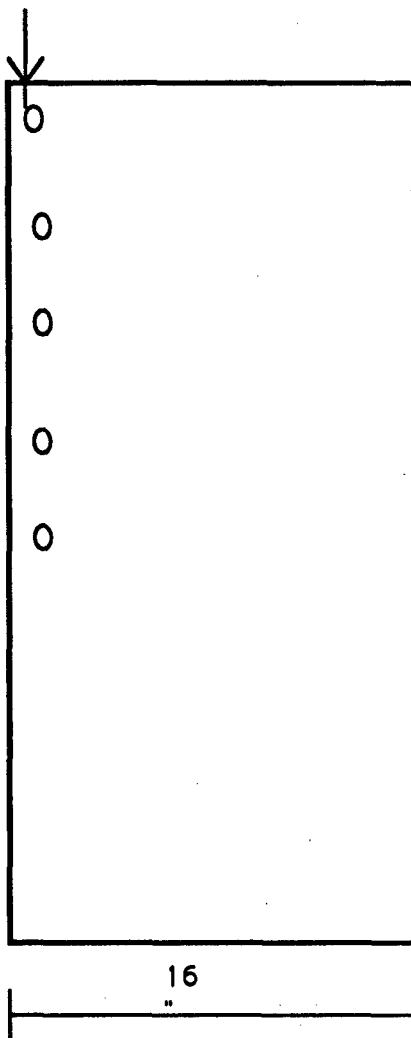
# BACK-PLATE

CENTER OF CLEARANCE HOLES .375" FROM THE LONGER SIDE

10 CLEARANCE HOLES ON BOTH SIDES OF THE BACK-PLATE AT .5", 5", 10", 15", 20", 26", 32", 37", 42", 47" FROM THE TOP-- S.S. 1/2" S.H.C.S. SCREWS

BACK PLATE IS SCREWED ONTO THE FRAME THROUGH THESE 20 HOLE POSITIONS.

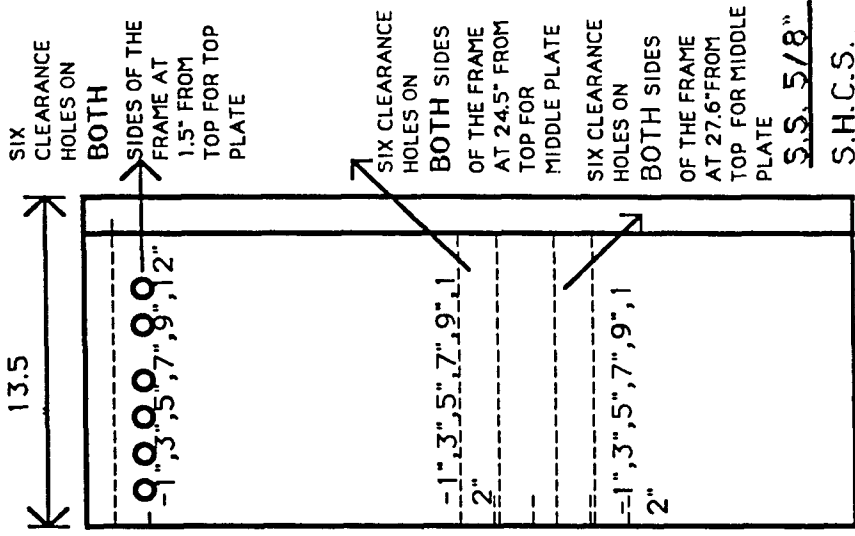
CORRESPONDING THREADS SHOULD BE TAPPED IN THE FRAME.



S.S. 1/2"  
S.H.C.S. SCREWS

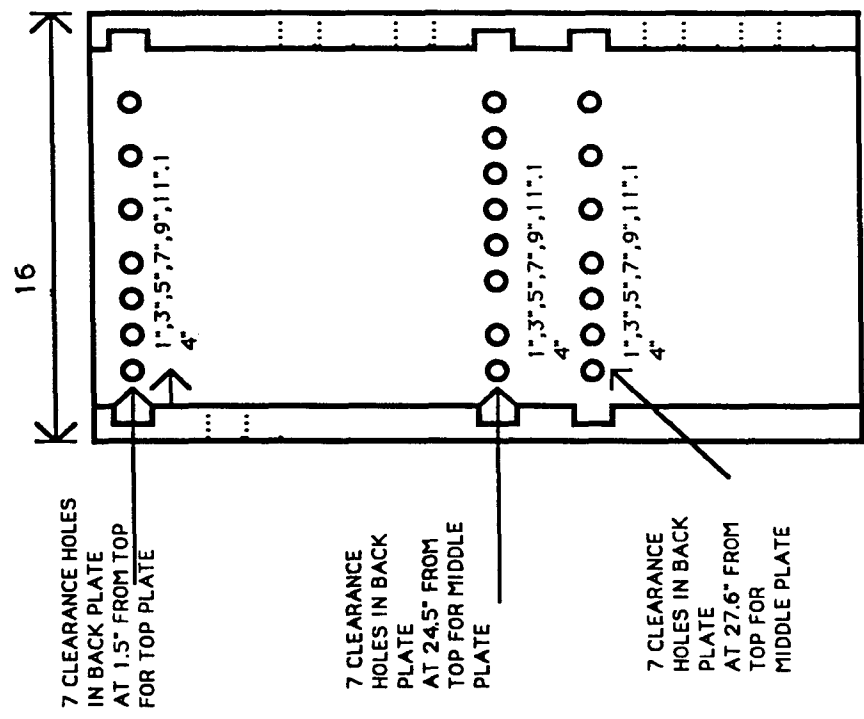
NOT  
DRAWN  
TO  
SCALE

FOR OTHER CLEARANCE HOLES, PL. REFER TO THE DRAWING FOR 'FRAME AND BACKPLATE'



R.H.S VIEW

NOT DRAWN TO SCALE



FRONT VIEW

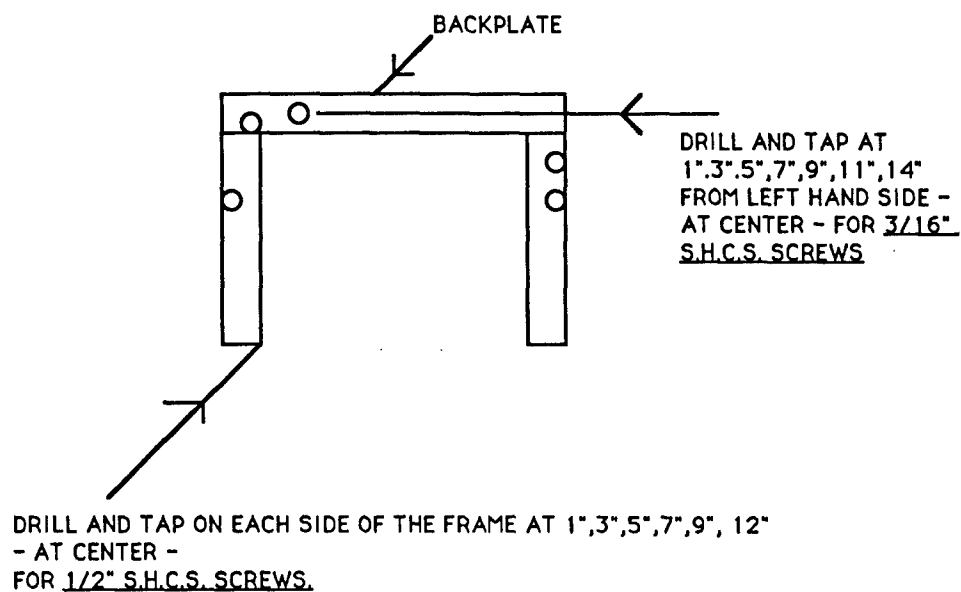
1. ONLY ONE VIEW OF THE HOLES IS SHOWN.  
2. OTHER SCREW POSITIONS ARE SHOWN IN NEXT DRAWING

Hole pattern in the frame and the back plate

S.S. 5/8"  
S.H.C.S.

SCREWS

BOTTOM VIEW OF THE FRAME AND THE BACKPLATE

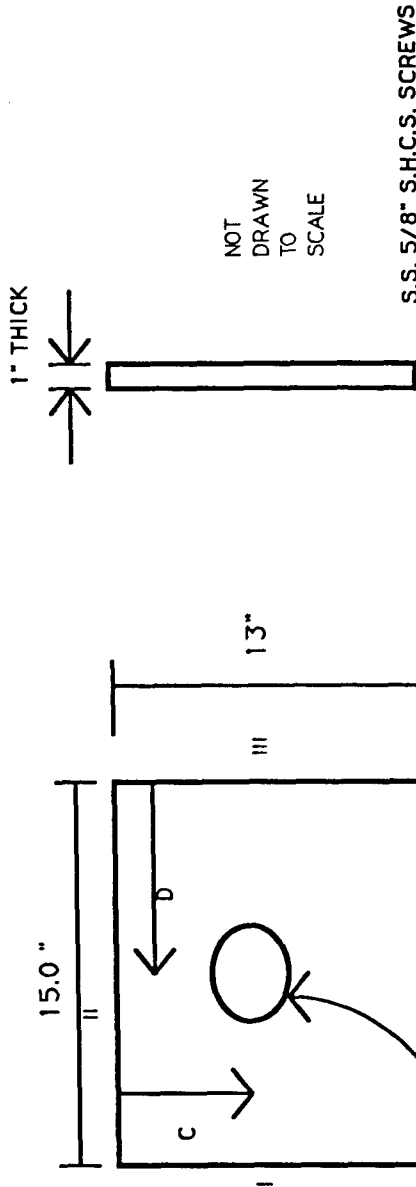


NOT DRAWN TO SCALE

S.S. 1/2" AND 3/16"  
S.H.C.S. SCREWS

THE THREADS SHOULD BE TAPPED ON SIDES I AND III TO MATCH THE CLEARANCE HOLES ON THE FRAME FOR THE TOP PLATE - FOR 5/8" S.H.C.S. SCREWS

THE THREADS SHOULD BE TAPPED ON THE SIDE II TO MATCH THE CLEARANCE HOLES ON THE BACK PLATE FOR THE TOP PLATE - FOR 5/8" S.H.C.S. SCREWS



CLEARANCE HOLE FOR 2 7/8" PIPE ( TOP PART OF SCREW JACK)- CLOSE FIT

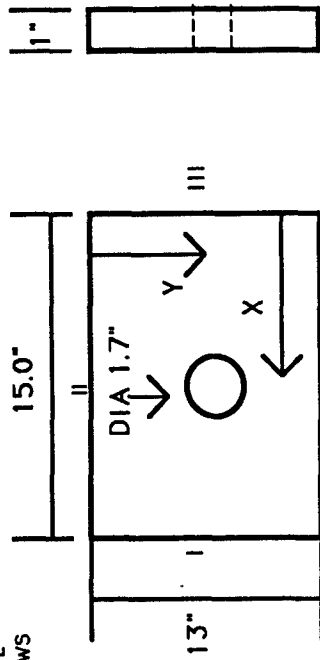
DIMENSIONS C AND D WOULD DEPEND UPON THE POSITION OF TOP PART OF THE SCREW JACK. THUS THE BIG CLEARANCE HOLE SHOULD BE DRILLED ONLY AFTER DECIDING THE POSITION OF THE SCREW JACK (WHICH WOULD BE BOLTED ONTO THE TOP PLATE).

TOP-PLATE

THE THREADS SHOULD BE TAPPED ON SIDES I AND III TO MATCH THE CLEARANCE HOLES ON THE FRAME FOR THE MIDDLE PLATE - FOR 5/8" S.H.C.S SCREWS

QUANTITY --- TWO

NOT DRAWN TO SCALE



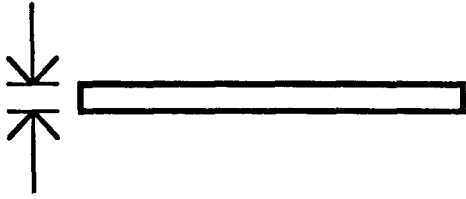
THE THREADS SHOULD BE TAPPED ON THE SIDE II TO MATCH THE CLEARANCE HOLES ON THE BACK PLATE FOR THE MIDDLE PLATE - FOR 5/8" S.H.C.S SCREWS

S.S. 5/8" S.H.C.S. SCREWS

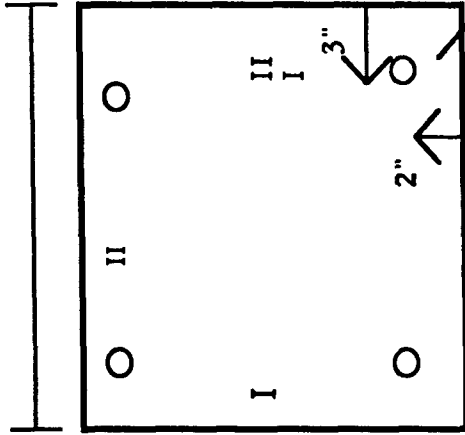
X AND Y DIMENSIONS: THE HOLE CENTER SHOULD BE CONCENTRIC WITH THE SCREW OF THE SCREW JACK.  
 THE HOLE SHOULD BE DRILLED AFTER THE INSTALLATION OF THE SCREW JACK IN THE TOP PLATE

MIDDLE-PLATE

0.50" THICK



16"



13.5"

THE CLEARANCE HOLES (6 ON EACH SIDE) ON SIDES I AND III TO MATCH THE THREADS ON THE FRAME FOR THE BOTTOM PLATE - FOR 1/2" S.H.C.S. SCREWS

7 CLEARANCE HOLES ON THE SIDE II TO MATCH THE THREADS ON THE BACK PLATE FOR THE BOTTOM PLATE- FOR 3/16" S.H.C.S

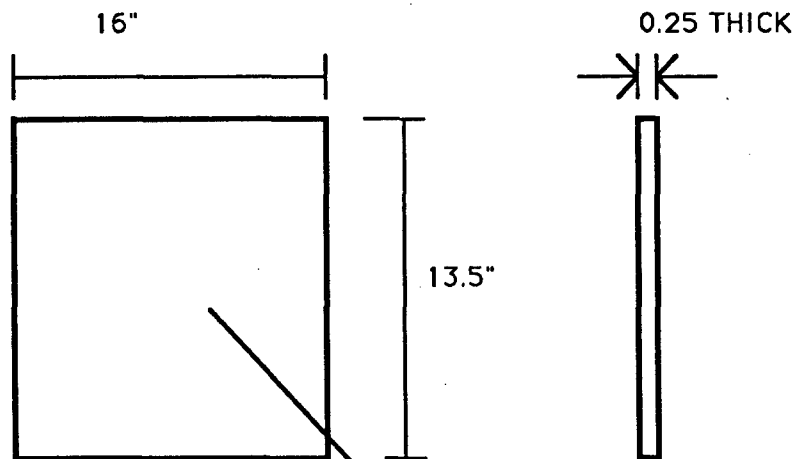
NOT DRAWN TO SCALE

FOUR CLEARANCE HOLES FOR ATTACHMENT TO THE SECOND BOTTOM PLATE (FOR 3/16" S.H.C.S SCREWS)

S.S. 1/2" AND 3/16" S.H.C.S. SCREWS

FIRST BOTTOM-PLATE

SECOND BOTTOM-PLATE



S.S. 3/16" S.H.C.S.  
SCREWS

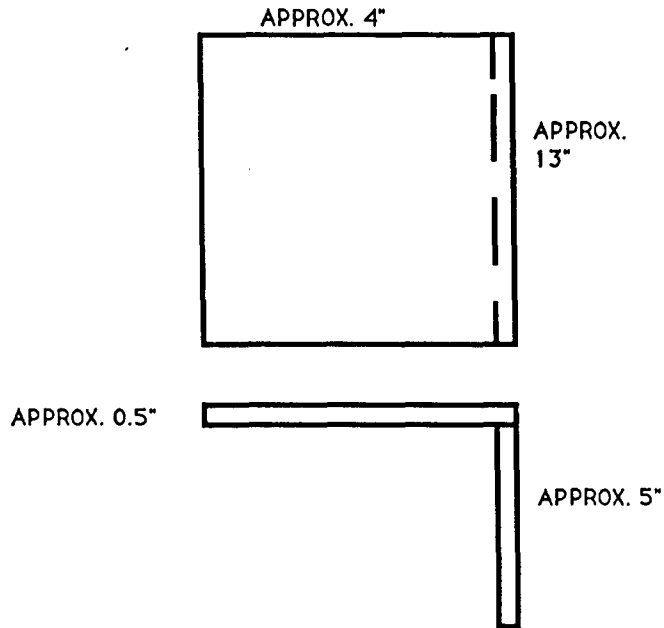
DRILL AND TAP AT FOUR POSITIONS CORRESPONDING  
TO THE CLEARANCE HOLES IN THE FIRST BOTTOM PLATE  
- FOR 3/16" SCREWS

Material of construction : TEFLON

NOT  
DRAWN  
TO  
SCALE

SUPPORT

Material of construction :  
ALUMINIUM (ANY KIND)



THE SUPPORT WOULD HOUSE THE GEAR REDUCER AND THE MOTOR, THE DIMENSIONS SHOULD BE CHOSEN ACCORDINGLY. THE MOTOR WOULD BE COUPLED TO THE GEAR REDUCER WHICH INTURN WOULD BE COUPLED TO THE INPUT SHAFT OF THE SCREW JACK (INSIDE THE FRAME).

NOT  
DRAWN  
TO  
SCALE

- 1.THE TWO PARTS OF THE SUPPORT SHOULD BE BOLTED TOGETHER.
- 2.THE SUPPORT SHOULD BE BOLTED TO THE FRAME.

**APPENDIX B**  
**Coagulation of an isotropic PBZT/MSA solution in various**  
**non-solvents (Ref. 38)**

Table B-1 Coagulation rates for an isotropic PBZT/MSA solution in various non-solvents (ref. 38).

Coagulant	Coagulation rate $\gamma/\sqrt{t}$ ( $\mu\text{sec}^{-1}$ )
H <sub>2</sub> O	63.1
20% MSA/H <sub>2</sub> O	41.0
30% " "	32.4
40% " "	21.2
50% " "	15.5
MeOH	50
3% MSA/MeOH	35 ~ 39
10% " "	25.8 ~ 26.6
20% " "	23.2 ~ 25.2
30% " "	20.4 ~ 23.9
40% " "	18.2 ~ 20.2
50% " "	16.3
60% " "	15.2
5% MeOH/xylene	(incomplete coag.)
10% " "	19.4
10% MeOH/CHCl <sub>3</sub>	(incomplete coag.)
10% MeOH/triethanolamine	9.0
50% MeOH/triethanolamine	18.4
C <sub>2</sub> H <sub>5</sub> OH	27.0
n-propanol	-
10% MSA/C <sub>2</sub> H <sub>5</sub> OH	16.8
20% " "	16.1
glycerol	5.7
triethanolamine	8.2
50% MeOH/glycerol	11
50% MeOH/CHCl <sub>3</sub>	25.4